JOURNAL OF GEOPHYSICAL RESEARCH, VOL. 98, NO. C7, PAGES 12,579–12,600, JULY 15, 1993

Spectral Characteristics of Time-Dependent Orbit Errors in Altimeter Height Measurements

DUDLEY B. CHELTON AND MICHAEL G. SCHLAX

College of Oceanography, Oregon State University, Corvallis

A mean reference surface and time-dependent orbit errors are estimated simultaneously for each exact-repeat ground track from the first two years of Geosat sea level estimates based on the Goddard Earth model (GEM)–T2 orbits. Motivated by orbit theory and empirical analysis of Geosat data, the time-dependent orbit errors are modeled as 1 cycle per revolution (cpr) sinusoids with slowly varying amplitude and phase. The method recovers the known "bow tie effect" introduced by the existence of force model errors within the precision orbit determination (POD) procedure used to generate the GEM-T2 orbits. The bow tie pattern of 1-cpr orbit errors is characterized by small amplitudes near the middle and larger amplitudes (up to 160 cm in the 2 years of data considered here) near the ends of each 5- to 6-day orbit arc over which the POD force model is integrated. A detailed examination of these bow tie patterns reveals the existence of daily modulations of the amplitudes of the 1-cpr sinusoid orbit errors with typical and maximum peak-to-peak ranges of about 14 cm and 30 cm, respectively. The method also identifies a daily variation in the mean orbit error with typical and maximum peak-to-peak ranges of about 6 cm and 30 cm, respectively, that is unrelated to the predominant 1-cpr orbit error. It is suggested that the two daily signals arise from daily adjustments of the drag coefficient in the GEM-T2 POD procedure. Application of the simultaneous solution method to the much less accurate Geosat height estimates based on the Naval Astronautics Group orbits concludes that the accuracy of POD is not important for collinear altimetric studies of time-dependent mesoscale variability (wavelengths shorter than 1000 km), as long as the time-dependent orbit errors are dominated by 1-cpr variability and a long-arc (several orbital periods) orbit error estimation scheme such as that presented here is used. The accuracy of POD becomes more important for studies of larger-scale variability.

1. INTRODUCTION

Estimation of sea surface height by satellite altimetry is straightforward in principle. In practice, however, altimetry is possibly the most complicated of all oceanographic observational techniques. The range between the antenna and the sea surface is determined from the two-way travel time of short pulses of microwave radiation transmitted by the altimeter. As described by *Chelton et al.* [1989], the technical details of the measurement technique are very complex. Moreover, in addition to a host of instrumental corrections, the range estimate computed from two-way travel time must be corrected for the refractive effects of atmospheric water vapor, dry gases, and ionospheric electrons and a sea state bias that arises because of the presence of waves on the sea surface. These environmental corrections are described in detail by *Chelton* [1988] and are not addressed here. That the range can be estimated to an accuracy of better than one part in 10^7 from an orbit height of about 1000 km is remarkable. However, even if the range could be measured perfectly, the range measurements alone are not sufficient for oceanographic applications. In order to convert a range estimate to sea surface height relative to a reference ellipsoid approximation of the Earth's surface (the reference surface traditionally used in satellite altimetry), the height of the satellite above the same reference ellipsoid must be estimated independently and subtracted from the range measurement. If neglected, errors in orbit height estimates can render altimeter data essentially useless for many purposes.

Paper number 93JC00721.
0148-0227/93/93JC-00721$05.00

Estimates of the orbit height as a function of time are obtained through precision orbit determination (POD) techniques based upon a sophisticated force model constrained by irregularly spaced satellite tracking measurements [e.g., *Tapley*, 1989; *Wagner*, 1989]. Root-mean-square (rms) accuracies as good as 20 cm have been quoted for the Geosat orbit inclination and 800 km altitude when altimeter data are included in the gravity model and in the POD [*Marsh et al.*, 1990*a*]. However, orbit height determination based on the more traditional (and less controversial) fitting of model estimates to tracking data without the use of altimeter data is generally considered to have an rms accuracy of about 30–50 cm for Geosat, primarily because of the sparse geographical coverage and low accuracy of the tracking data available for the unclassified Geosat data [e.g., *Haines et al.*, 1990; see also B. J. Haines et al., Application of the GEM-T2 gravity model to altimetric satellite orbit computation, submitted to *Journal of Geophysical Research*, 1993, hereinafter referred to as Haines et al., submitted]. (A notable exception is *Shum et al.* [1990], who report an accuracy of ~20 cm using 17-day orbit arcs.) Time series of raw altimeter data for a particular location along a repeating ground track are thus effectively equivalent to a dense grid of tide gauge measurements sampled infrequently (between a few days and a few weeks, depending on the satellite orbit configuration) with 30–50 cm noise.

With continued improvements in POD force models, expanded geographical coverage and improved accuracy of satellite tracking data and a higher orbit altitude of 1300 km, orbit height uncertainties are expected to decrease to less than 13 cm for the TOPEX/Poseidon altimetric satellite launched in August 1992. Evidence that such POD accuracy is feasible has been presented by *Tapley et al.* [1990] and *Sanchez* [1991]. Preliminary analyses of

TOPEX/Poseidon orbits confirm the anticipated ~ 10-cm orbit accuracy. Although this orbit accuracy is extremely impressive, it is still (by a factor of 3 or more) the single largest source of error in altimetric estimates of sea surface height. These residual orbit errors must be removed for studies of all but the most energetic oceanographic phenomena.

The objective of this study is to investigate in detail the characteristics of residual orbit errors pertinent to altimetric studies of time-dependent sea level variability. The data used for this purpose consist of 2 years of 17-day exact repeat Geosat estimates of sea surface height (43 repeat cycles beginning November 8, 1986) based on two different POD estimates of orbit height: the relatively low accuracy NAG operational orbits (~350 cm rms error) produced by the Naval Astronautics Group (Appendix A) and the much more precise Goddard Earth model (GEM)–T2 orbits (~40 cm rms accuracy) produced by the Goddard Space Flight Center (Appendix B).

A summary of orbit error characteristics is given in section 2. A brief overview of methods used to estimate orbit errors and a detailed description of the method used in this study are given in section 3. The method is applied to the GEM-T2 Geosat data and the results are interpreted in section 4. The method is also applied to the NAG Geosat data in order to ascertain the importance of POD accuracy for altimetric studies of time-dependent sea level variability. The separate GEM-T2 and NAG residual height data sets after removal of the respective orbit error estimates are compared in section 5.

2. Characteristics of Orbit Errors

The problem of radial orbit error in satellite altimetry is well recognized. Virtually every published application of altimeter data devotes some discussion to the method used by that particular study to mitigate the effects of orbit error. To first order, the Earth's gravity field can be considered spherically symmetric, which results in elliptical satellite orbits [*Kaula*, 1966]. Numerous theoretical studies have shown that uncertainties in the orbital eccentricity, semimajor axis and period all lead to errors in estimates of the radial distance between the centers of mass of the Earth and satellite that are dominated by sinusoidal variability at the orbital period [e.g., *Colombo*, 1984; *Wagner*, 1985, 1989; *Tapley and Rosborough*, 1985; *Engelis*, 1988; *Schrama*, 1989]. The amplitude and phase of the 1–cycle per revolution (cpr) sinusoidal time-dependent orbit errors vary slowly with time. Because repeat samples of a given ground track are separated by many orbits (244 for the Geosat 17-day repeat period), the amplitude and phase of the time-dependent orbit errors along the track can be assumed to be essentially random from one repeat cycle to the next.

An obvious approach to verification of the 1-cpr character of time-dependent orbit errors is to compute the frequency spectrum of the altimetric height data, after removal of the geoid and other time-invariant contributions, from long data arcs spanning multiple orbital revolutions. The large data gaps over land that occur during each satellite orbit lead to practical difficulties with traditional spectral analysis methods. A crude (but effective for present purposes) procedure was used here. Along each ground track, the height measurements over water were interpolated to a regular grid with approximately 7-km spacing. At each grid location, the arithmetic average height over the 22 repeat cycles during the first year of Geosat data was subtracted from each repeat sample of the grid point. (Limitations of this method of estimating a mean height profile are discussed below; for present purposes, however, the pointwise arithmetic mean is adequate.) This average height includes the time-invariant geoid and dynamic sea level associated with the 12-month mean ocean circulation, as well as any systematic time-invariant components of orbit error. The resulting time-variable height data were then simultaneously low-pass filtered to resolve length scales longer than 10,000 km (one quarter of an orbit) and interpolated to an evenly spaced grid of eight samples per orbit using a quadratic loess smoother. This interpolation algorithm and its filtering characteristics are described in detail by *Cleveland and Devlin* [1988], *Chelton et al.* [1990] and *Schlax and Chelton* [1992]. The choice of a 10,000-km cutoff was dictated by the expectation that time-dependent orbit errors have very little energy at frequencies higher than about 4 cpr. This is also about the shortest resolvable length scale that makes sense for interpolation of altimeter data across large continental land masses.

The spectra of the filtered and interpolated time-dependent GEM-T2 and NAG height data are shown in Figure 1. For both data sets, the Geosat height variability is dominated by energetic variability concentrated at a frequency of 14.3 cycles per day (cpd), which corresponds to the orbital period of 101 min. In addition to this spectral peak at 1 cpr, there is a small peak at 2 cpr in the GEM-T2 spectrum and at 3 cpr in both spectra, but the narrow-band variabilities at these higher frequencies are less energetic by 2–3 orders of magnitude than the variability at 1 cpr. At lower frequencies, there are identifiable spectral peaks at 1 cpd and 2 cpd in the GEM-T2 spectrum. The spectral energies at these lower frequencies are smaller than the dominant 1-cpr variability by 1.5 orders of magnitude but are nonetheless statistically significant. The daily variability associated with these 1- and 2-cpd spectral peaks is discussed in section 4.3.

The approximate factor-of-20 difference between the energies of the orbit errors in the NAG and GEM-T2 data sets is indicative of the much larger orbit error amplitudes in the NAG data. The rms orbit errors within the frequency band centered at 1 cpr inferred from the spectra in Figure 1 are 99.6 and 10.7 cm for the NAG and GEM-T2 data sets, respectively. These values account for two thirds and one third, respectively, of the total variances of the spectra in Figure 1, which are consistent with the total time-dependent rms orbit error estimates of 120.3 and 20.7 cm over all frequencies deduced independently from crossover differences for each 1-year data set after removal of the pointwise arithmetic mean.

A noteworthy feature of the spectrum of GEM-T2 data in Figure 1*a* is the splitting of the primary 1-cpr spectral peak. A detailed examination reveals that the closest peaks on each shoulder of the central peak both differ from the 1-cpr frequency of the central peak by exactly 1 cpd. A similar splitting of the 1-cpr spectral peak has previously been found by *Wunsch* [1991]. These sum and difference energetic variabilities are indicative of an amplitude modulation of the fundamental 1-cpr orbit error with a 24-hour periodicity. More convincing evidence for

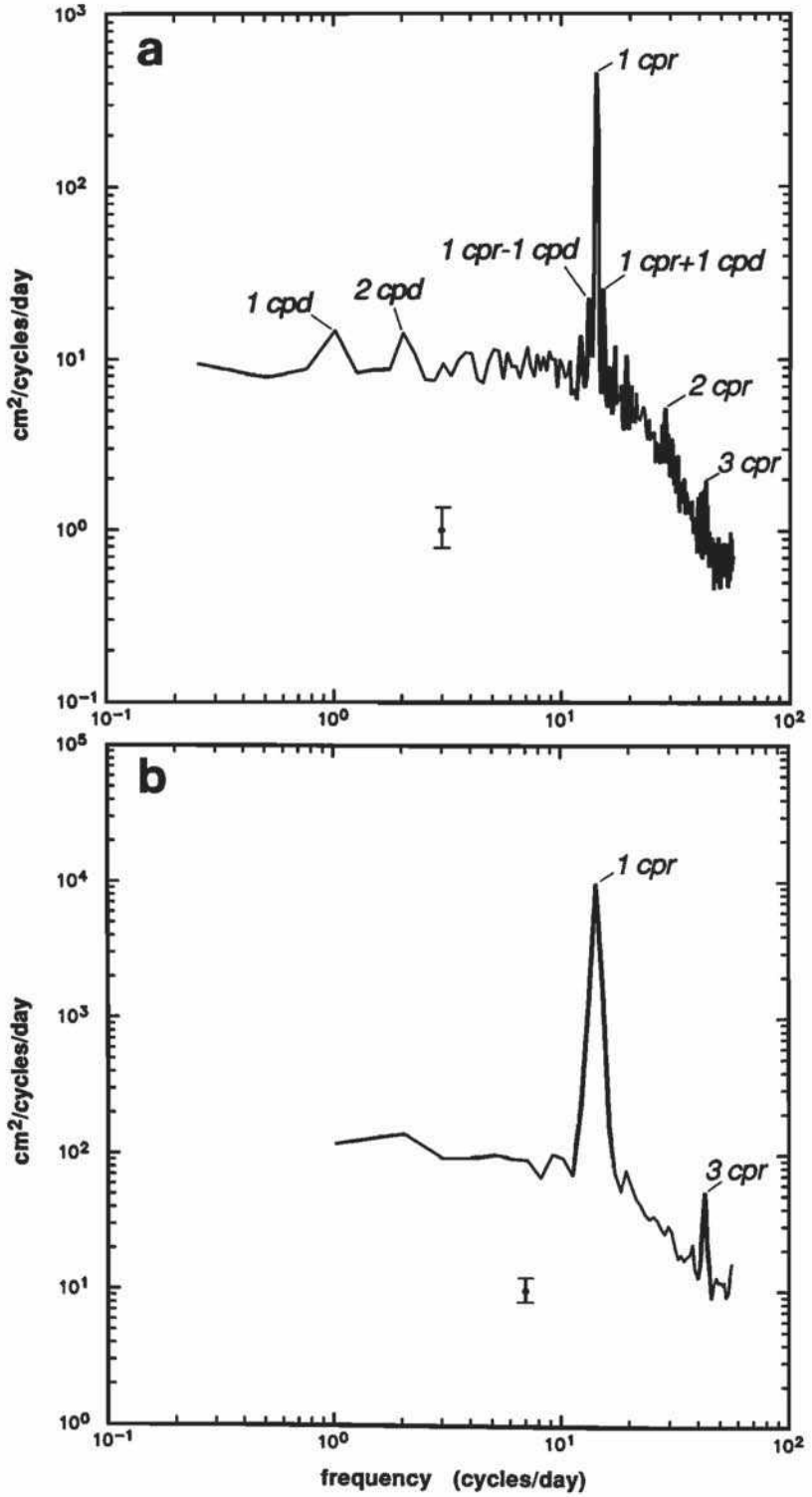

Fig. 1. Power spectral density of time-varying Geosat sea surface height estimates from the first year of the Exact Repeat Mission beginning November 8, 1986, based on (*a*) the GEM-T2 orbits, and (*b*) the NAG orbits. These smoothed spectra were obtained by ensemble averaging the individual spectra with 2 degrees of freedom over all POD orbit arcs spanning a period of 4 days or longer for the GEM-T2 data and 24 hours or longer for the NAG data. The error bars represent 95% confidence intervals.

a daily modulation of the amplitude of 1-cpr variability is given in section 4.2.

A splitting of the primary 1-cpr spectral peak is not evident in the spectrum of NAG data in Figure 1*b*. As is described in appendices A and B, the NAG orbits are based on 24-hour orbit arcs, compared with the 5- to 6-day orbit arcs used for the GEM-T2 orbits. If a 24-hour modulation of the 1-cpr variability existed in the NAG data, it would not be resolvable in 24-hour data arcs. Similarly, the NAG orbit arcs are too short to resolve the 1-cpd and 2-cpd

spectral peaks evident in the GEM-T2 data.

Irregularities in the distribution of mass within the Earth introduce perturbations that cause the satellite orbit to deviate from the elliptical orbit that would exist if the gravity field were spherically symmetric. These gravitationally induced perturbations are very complex as sampled along the satellite ground track, resulting in a broad-banded series of line spectra in time series constructed from data along the satellite ground track [e.g., *Tapley and Rosborough*, 1985; *Rosborough and Tapley*, 1987; *Rosborough and Marshall*, 1990; *Haines et al.*, 1990; *Shum et al.*, 1990; *Sirkes and Wunsch*, 1990]. Neglecting the comparatively small orbit errors associated with time-varying gravitational effects such as tides and with the slow precession of the mean argument of perigee of the orbit, gravitationally induced orbit errors are the same for each repeat sample of a given ground track in an exact repeat orbit configuration. Thus although they appear time-dependent as sampled by the satellite, the static components of gravitationally induced orbit errors are actually only spatially dependent and can be considered time-invariant at a given location in collinear data. This contribution to the total orbit error is therefore quite distinct from the 1-cpr time-dependent orbit errors introduced by uncertainties in the orbital parameters.

It should be apparent that the time-invariant gravitationally induced orbit errors cannot be distinguished from the time-invariant geoid and mean ocean circulation contributions to the altimetric estimates of sea level. These time-independent signals are all eliminated from collinear data when the time-averaged height profile is removed from each repeat track of data, resulting in residual height data with the much simpler time-dependent orbit errors dominated by 1-cpr variability (Figure 1; see also *Wunsch* [1991]).

When using altimeter data to estimate the general circulation, the total orbit error (time-invariant plus time-dependent) must be removed from the data. This is a serious problem, since it is very difficult to distinguish time-invariant orbit error from the time-invariant contribution to sea surface height and errors in the geoid. A method of estimating the total orbit error using an analytical technique which simultaneously improves the geoid and orbit model has been developed and applied to GEM-T1 data by *Denker and Rapp* [1990]. The method has more recently been applied to GEM-T2 data by *Rapp et al.* [1991].

The vast majority of applications of altimeter data are interested in the time-dependent mesoscale and large-scale variability of sea surface topography and therefore require estimates of only the time-dependent component of orbit error. The orbit error associated with the static component of the gravity field is removed along with the mean sea level (including the geoid) prior to analysis of exact repeat altimeter data for studies of sea level variability. The characteristics of the time-dependent component of orbit error that affect all oceanographic applications of altimeter data are examined in detail in this study.

3. Orbit Error Estimation

Many methods have been used to estimate time-dependent residual orbit errors in altimeter data. They all capitalize on the long-wavelength characteristic of this component of orbit error. The standard procedure for estimating orbit error from exact repeat altimeter data is a sequential method that begins by interpolating the collinear data onto a regular grid along the satellite ground track and removing the pointwise arithmetic mean sea level from every repeat sample at each grid point. Provided that an adequate number of repeat cycles are available, this procedure very effectively eliminates the marine geoid and time-invariant orbit error contributions to the altimeter estimates of sea surface elevation. The predominantly 1-cpr time-dependent orbit error in the residual data is then approximated by a least squares fit to an analytical functional form over data arcs of typically a few thousand kilometers.

The most common functional approximations of the time-dependent orbit error are low-order polynomials [e.g., *Rummel and Rapp*, 1977; *Anderle and Hoskin*, 1977; *Douglas and Goad*, 1978; *Rapp*, 1979; *Douglas and Gaborski*, 1979; *Cheney and Marsh*, 1981; *Cheney et al.*, 1983; *Zlotnicki et al.*, 1989; *Le Traon et al.*, 1990; *Cheney and Miller*, 1990]. In practice, polynomials higher than second order (quadratic) are seldom used, and a first-order polynomial (the so-called "bias and tilt correction") is the form used most often.

For a given polynomial order, the accuracy of a polynomial approximation for the fundamentally sinusoidal time-dependent orbit error worsens with increasing data arc length. Moreover, *Sandwell and Zhang* [1989], *Tai* [1989], *LeTraon et al.* [1991], and *van Gysen et al.* [1992] have all noted that polynomial orbit error fits over long data arcs can introduce spurious sea level variability near the ends of the data arcs. As the arc length decreases, however, a given order of polynomial approximation increasingly "overfits" the data and removes more of the oceanographic signal of interest. For example, *Cheney and Miller* [1990] found that quadratic polynomial adjustments over arc lengths of 2000–3000 km remove more than half of the oceanographic signal in the western tropical Pacific. The trade-offs between the adequacy of the polynomial approximation of the orbit error and attenuation of the signal because of polynomial overfitting have been investigated in detail by *Tai* [1989, 1991] and *Le Traon et al.* [1991].

A rule of thumb that has become more or less accepted standard practice is that bias and tilt adjustments should be used for arc lengths shorter than 1500 km and quadratic adjustments should be used for arc lengths longer than 2500 km. These forms of orbit error correction may be adequate for altimetric studies of mesoscale variability, but they are not well suited to studies of basin-scale variability. With ample computing power now readily available, there is no need to limit orbit error estimation to arc lengths of a few thousand kilometers. Consequently, an increasing number of recent studies have modeled the orbit error as a least squares fit over arc lengths of half an orbit (about 20,000 km) or longer. The most appropriate orbit error model over such long arc lengths is a 1-cpr sinusoid [e.g., *Sanchez and Cartwright*, 1988; *Tai*, 1988*b*; *Chelton et al.*, 1990; *Cartwright and Ray*, 1990; *Wagner*, 1990; *Denker and Rapp*, 1990]. As in the case of high-order polynomial approximations, sinusoidal fits over short data arcs can remove much of the signal of interest. Reliable estimates of the sinusoidal approximation of orbit error require data arcs of the order of half an orbit or longer.

An obvious limitation of a 1-cpr orbit error correction procedure is that any time-dependent oceanographic signal characterized by 1 cpr is removed along with the principal orbit error. Fortunately, most ocean signals of interest do not have such long length scales. A notable exception is the very large scale steric sea level change associated with seasonal hemispheric heating and cooling. Most of this ocean signal is unfortunately sacrificed in the elimination of the 1-cpr variability. This hemispheric signal is less interesting scientifically than the sea level changes that occur on much shorter spatial scales in association with seasonal variations in the ocean circulation.

A problem common to all sequential solution methods of orbit error estimation is the requirement for an accurate estimate of mean sea level in order to isolate the time-dependent component of orbit error in the altimeter range measurements. As was discussed extensively by *Chelton et al.* [1990], this is especially a problem with the NAG Geosat data. The passive gravity gradient stabilization that controlled the orientation of the Geosat satellite resulted in frequent attitude excursions beyond tolerable limits, leading to significant data loss. Because of the large amplitudes of NAG orbit errors, estimates of the arithmetic mean sea level can be statistically unstable at any grid location where there are data dropouts during one or more of the repeat cycles of data. The problem of unreliable arithmetic mean sea level estimates is reduced with more accurate POD such as the GEM-T2 orbits but can still be significant when there are frequent data dropouts.

A method of dealing with the problem of unstable estimates of mean sea level has recently been developed by *van Gysen et al.* [1992]. The method uses a least squares technique to estimate simultaneously a profile of mean sea level along a ground track and an orbit error estimate for each repeat cycle of the ground track. The mean sea level profile obtained in this manner is entirely consistent with the chosen modeling of the orbit error. Any analytical form for the orbit error model can be used; *van Gysen et al.* [1992] recommend using a sinusoid model, even for short data arcs. They use quarter-revolution data arcs (about 10,000 km) but suggest that full-revolution data arcs would be preferable in order to reduce the risk of eliminating long-wavelength ocean signal in the least squares fit to a sinusoid.

The simultaneous solution method is summarized in some detail here in order to establish a notation for describing the enhancements that have been added to the method in this study. Consider a single track of data, defined to be a data arc between the maximum poleward latitudes sampled by the altimeter (south to north for an ascending track and north to south for a descending track). The maximum latitudes sampled by Geosat were about 72°. The simultaneous solution method requires a fixed sampling grid along each track. This was achieved by interpolating the 1-s average Geosat data along each track to 2345 grid locations x_j between 65°S and 65°N, uniformly spaced in angular displacement ω_j relative to the equatorial crossing along the track [*Zlotnicki et al.*, 1990]. This corresponds to an along-track grid spacing of approximately 7 km.

The sea level measurement at location x_j at the time of the ith repeat pass along the track of data under consideration can be decomposed as

$$h_i(x_j) = \overline{h}(x_j) + h_i'(x_j) + e_i'(x_j), \tag{1}$$

where $\overline{h}(x_j)$ is the time-invariant component of $h_i(x_j)$ over all repeat passes, $h_i'(x_j)$ is the time-dependent sea level estimate during pass i and $e_i'(x_j)$ is the time-dependent component of orbit error for pass i. For the 43 repeat cycles of Geosat data considered here, the repeat pass index i ranges from 1 to $N = 43$. The time-invariant signal $\overline{h}(x_j)$ over the duration of the data set (which will be referred to here as the "mean sea level") includes the marine geoid, the time-invariant orbit error, and the time-invariant dynamic sea level associated with the mean ocean circulation. The time-dependent sea level estimate $h_i'(x_j)$ for pass i includes the dynamic sea level signal of interest to oceanographic applications as well as time-dependent components of measurement error from inaccuracies in environmental corrections, ocean tides, and the sea state bias correction.

The term in (1) that is of interest to this study is the time-dependent component of orbit error, which is modeled here for pass i as

$$e_i'(x_j) = a_i + b_i \sin\omega_j + c_i \cos\omega_j, \tag{2}$$

corresponding to a 1-cpr sinusoid and a constant offset. It is straightforward to extend this model to include higher harmonics of 1 cpr or any other analytical expressions. However, as measured by the rms crossover differences of residual height data after removal of the estimated orbit errors, no significant improvement in orbit error estimation was obtained with the Geosat GEM-T2 data when (2) was expanded to include a 2-cpr sinusoid. This supports the conclusion drawn from Figure 1*a* that there is little orbit error energy at any harmonics other than 1 cpr. Note that just like the sequential methods, removal of 1-cpr variability by the simultaneous solution method sacrifices very large scale ocean signals such as the steric effects of seasonal hemispheric heating and cooling.

Orbit errors were assumed to vary slowly enough that the three orbit error parameters a_i, b_i, and c_i could be assumed constant for each pass of a given ground track. By performing a separate least squares analysis for each successive pass (half orbit) of data, orbit errors were allowed to vary temporally from one pass to the next. The simultaneous solution for a given track uses data from all repeat passes of the track to estimate the mean sea level $\overline{h}(x_j)$ over all passes and the three orbit error parameters in (2) for each individual repeat pass. For the ith pass of data, the equations (1) and (2) at the 2345 grid locations x_j can be expressed in matrix form as

$$\mathbf{h}_i = \overline{\mathbf{h}} + \mathbf{A}\mathbf{x}_i + \mathbf{h}_i', \tag{3}$$

where $\mathbf{x}_i$ is a 3×1 column vector consisting of the orbit error parameters a_i, b_i, and c_i to be estimated, $\mathbf{A}$ is the 2345×3 matrix of orbit error model coefficients with jth row consisting of the three elements $(1, \sin\omega_j, \cos\omega_j)$ and $\mathbf{h}_i$, $\overline{\mathbf{h}}$, and $\mathbf{h}'$ are 2345×1 column vectors of total sea level, mean sea level, and time-dependent sea level, respectively. There is one such equation for each of the N passes of a given track, with $\overline{\mathbf{h}}$ and $\mathbf{A}$ the same for all passes.

The details for solving the underdetermined system of N

equations (3) using constrained least squares to estimate the $3N$ orbit error parameters contained in the N vectors $\mathbf{x}_i$ and the 2345 mean sea level values (excluding those grid points over land) contained in the vector $\overline{\mathbf{h}}$ are described by *van Gysen et al.* [1992]. The constraint applied here to overcome the rank deficit of the normal equations is that

$$\sum_{i=1}^{N} e_i'(x_j) = 0, \tag{4}$$

i.e., that the time-dependent orbit errors at each grid location x_j sum to zero over the N repeat passes of data. This is a sensible choice since the time-invariant orbit errors are included in the mean sea level $\overline{h}(x_j)$ estimated for each location x_j.

To assure slow variations in the estimates of the constant offset and the amplitude and phase of sinusoidal orbit error, the method of *van Gysen et al.* [1992] was extended to include data from adjoining tracks in a weighted least squares estimate of orbit error and mean sea level for each individual track. This procedure also reduces the problem of overfitting the data from passes interrupted by large land areas or from passes with extensive data dropouts.

The extended formalism can be summarized as follows. Define $\mathbf{h}_{in}$ to be the vector of sea level data from the ith pass of track n, with the track indices ordered sequentially in time. Denote the track under consideration by the index k. The orbit error parameters a_i, b_i, and c_i for track k are estimated from a data span of width $2s+1$ centered on track k, i.e., from $\mathbf{h}_{in}, n = k-s, \ldots, k+s$. Let ω_{jn}^k denote the angular displacement of the jth grid location of track n from the equatorial crossing of track k. In the weighted least squares estimation of orbit error parameters for track k, the weight applied to the altimeter height measurements from all repeat passes at this grid location is determined by the tricubic function

$$\begin{aligned} W_{jn}^k &= 1 && |\omega_{jn}^k| \le 3\pi/2; \\ W_{jn}^k &= \left[1 - \left(d_{jn}^k\right)^3\right]^3 && \text{otherwise;} \end{aligned} \tag{5}$$

where

$$d_{jn}^k = \frac{|\omega_{jn}^k| - 3\pi/2}{(s-1)\pi}. \tag{6}$$

The angular span of a single track is π. The weighting scheme (5) thus assigns a weight of 1 to all observations in track k and the adjacent track (half orbit) on each side of track k. More distant observations are smoothly downweighted to zero at an angular displacement of $\pm(s+1/2)\pi$, corresponding to the most distant observations within the data span of $2s+1$ tracks centered on track k.

The minimum resolvable time scale of variations in the amplitude and phase of the sinusoid orbit error estimate is controlled by the span of data used in the weighted least squares estimate. A large value of s results in very slow changes of the orbit error parameters. Smaller values of s allow shorter time scale variations in orbit error parameters. However, small values of s also increase the risk of overfitting the data and attenuating the large-scale ocean signal by the orbit error estimate. After some experimentation, a value of $s = 4$ was chosen for this study. The orbit error estimates for each pass of data are thus based on a total of nine consecutive passes (4.5 orbits) of data centered on the pass of interest. Any passes of data that fell outside of the POD orbit arc of the center pass were excluded from the weighted least squares fit. Orbit error estimates for passes within two orbits of the boundaries of each POD orbit arc are thus based on a weighted least squares fit to fewer than 4.5 consecutive orbits.

In practice, the quantity of data in the long data arcs used in the weighted least squares simultaneous estimation of mean sea level and orbit errors was unwieldy. For the purposes of orbit error estimation, many of the data are redundant. The volume of data was therefore reduced by an order of magnitude by including only every tenth grid location, corresponding to along-track intervals of about 70 km. The method thus yields an estimate of mean sea level only at every tenth grid location. After obtaining the simultaneous solutions at the decimated grid locations along each track, the mean sea level at each intermediate grid location was estimated as

$$\overline{h}(x_j) = \langle h_i(x_j) - \hat{e}_i(x_j) \rangle, \tag{7}$$

where $\hat{e}_i(x_j)$ is the estimated orbit error evaluated at grid location x_j from the sinusoid orbit error parameters obtained for pass i in the simultaneous solution. The angle brackets in (7) denote the arithmetic mean over all passes with nonmissing data at grid location x_j.

The orbit errors estimated in this manner by the simultaneous least squares solution may, in some cases, be overly influenced by data values at grid locations with high sea level variability. The concern is that the sinusoids may effectively overfit the data in high-variance regions because of the greater impact of "outlier data" in the least squares solution. This problem is discussed extensively by *Caruso et al.* [1990], *Kelly et al.* [1991], *Le Traon et al.* [1991], and *van Gysen et al.* [1992]. These studies recommend reducing the impact of energetic oceanographic variability on orbit error estimation by weighting the data at grid location x_j by the inverse of the height variance at that location.

In practice, the accuracies of estimates of sea level variability from raw altimeter data are limited by orbit error variance that for Geosat is as large as or larger than the sea level variance from mesoscale ocean variability. Although essentially equivalent results likely could have been obtained using simpler methods (e.g., using an a priori estimate of sea level variance from the global map produced by *Zlotnicki et al.* [1989]), an iterative reweighting scheme first suggested by *Caruso et al.* [1990] was used in this study to reduce the effects of orbit errors in the sea level variance estimates. In the first iteration, the orbit errors and mean sea level were estimated simultaneously with weights all taken as unity. The sea level variance at each location x_j was then computed after removal of these initial orbit error and mean sea level estimates. The simultaneous solution was then repeated once by weighting the data by the inverse of these initial variance estimates at each location. The details for implementing this procedure in the simultaneous least squares solution are described by *van Gysen et al.* [1992]. In the multitrack extended simultaneous solution method used here, the inverse variance weighting factors were scaled by the tricubic weights (5) applied to each grid location within

the span of data used in the least squares solution. Regions of large height variance along the satellite ground track are generally isolated geographically to short segments of the track and therefore seldom exert unduly large influence on the least squares solution over long (multiorbit) data arcs. The inverse variance weighting is therefore not generally a critical element of the orbit error estimation method.

4. GEM-T2 Orbit Errors

An example of the simultaneous solution method described in section 3 as applied to eight consecutive orbits during repeat cycle 19 of the GEM-T2 Geosat data is shown in Figure 2. The 1-cpr sinusoidal nature of the orbit error readily apparent in the raw data is typical of the 2 years of Geosat data considered here. It is also evident from this example that there is very little variance in the GEM-T2 data at any higher harmonics of the 1-cpr variability, again consistent with the spectral analysis in Figure 1*a*. This particular segment of data was chosen to illustrate the ability of the orbit error estimation technique to recover the abrupt change in amplitude and phase of the 1-cpr orbit error across the POD orbit arc boundary in the middle of the eight consecutive orbits.

The least squares fits of the modeled orbit errors (2) for sequential passes of data are equivalent to modeling the orbit error as

$$e'(t) = A(t) + B(t)\sin\left[\frac{2\pi t}{T} + \phi(t)\right], \qquad (8)$$

where T is the orbital period. Allowing for slow variations in the constant offset term $A(t)$ accommodates low-frequency variations in the orbit error with periods longer than the span of the weighted least squares fit used to estimate the orbit errors. Time series of the mean values $A(t)$ and the amplitudes $B(t)$ and phases $\phi(t)$ of 1-cpr GEM-T2 orbit error estimates (one estimate for each pass) for the first 22 cycles of the Geosat Exact Repeat Mission are shown in Figure 3. Slow variations in these orbit error parameters within each POD orbit arc, as well as abrupt changes across POD orbit arc boundaries, are clearly evident. (The more erratic appearance of the phase time series is just an artifact of the 360° circularity of the phase.) The characteristics of the orbit errors deduced from the time series of these parameters are described in this section.

4.1. *The Bow Tie Effect*

One of the most prominent features of Figure 3*a* is the generally larger orbit error sinusoid amplitudes $B(t)$ near orbit arc boundaries. This is a result of the POD iterative fit of selected force model scaling parameters and model-predicted satellite position and velocity to ground-based tracking data collected along the orbit arc. Because of the details of the POD least squares adjustment procedure used to generate the GEM-T2 orbits [see *Haines et al.*, 1990; Haines et al., submitted], estimates of orbit height tend to be most accurate near the middle of an orbit arc and become progressively degraded toward the ends of the arc. The resulting "bow tie" or "butterfly" pattern in residual orbit errors was apparently first noted theoretically and from orbit error simulations by *Colombo* [1984] (see also *Colombo* [1989]). Because the tracking data are not always uniformly distributed nor of uniform quality over the orbit arc, the minimum residual orbit error (the "knot" of the bow tie) can occur at points other than the center of the orbit arc. This is illustrated in Figure 4 by two examples of the orbit error estimates computed from the sinusoid amplitudes and phases in Figure 3. The knot occurs very near the middle of the orbit arc in Figure 4*a* but is closer to the beginning of the orbit arc in Figure 4*b*.

Another interesting feature of Figure 3*a* is that the maximum sinusoid orbit error amplitude within each POD orbit arc tends to be about 40 cm (corresponding to a peak-to-peak range of 80 cm) during the early period of the Geosat Exact Repeat Mission and increases to a maximum of about 90 cm (peak-to-peak range of 180 cm) toward the end of the 1-year record shown in the figure. The amplitudes of the bow tie patterns were even larger during the second year of the Exact Repeat Mission. This is evident in the time series of the maximum value of $B(t)$ in each orbit arc (i.e., the maximum of each bow tie pattern) shown in Figure 5*b*. Bow tie maxima were as large as

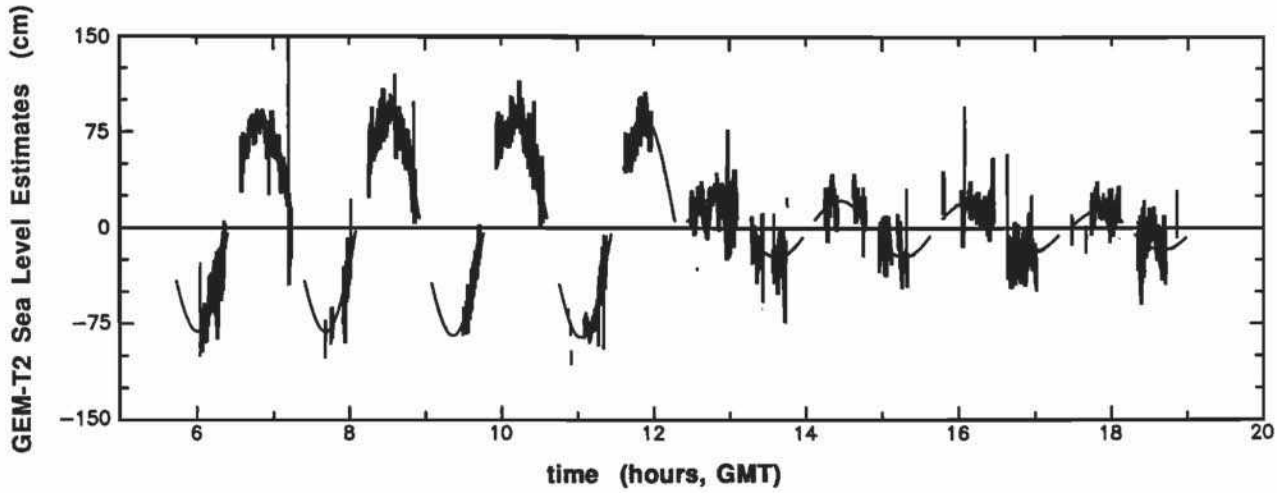

Fig. 2. Geosat height estimates with the time-invariant component removed (rough lines) for eight consecutive orbits on September 19, 1987, during cycle 19 of the Exact Repeat Mission. Estimates of the time-dependent 1-cpr orbit errors computed as described in the text with a span of 4.5 orbits are superimposed as the smooth lines. The abrupt change in the amplitude and phase of the sinusoidal orbit error after the fourth orbit coincides with the time of a GEM-T2 orbit arc boundary.

160 cm (peak-to-peak range of 320 cm) toward the end of the second year of data. Over the 2-year record, there are numerous short periods (up to a few months) of persistently large bow tie maxima. Superimposed on these short-period variations is an underlying secular increase over the 2-year period. This is almost certainly a consequence of drag errors in the POD force model from mismodeled variations in air density at the satellite orbit altitude.

In the generation of the GEM-T2 orbits, high-altitude atmospheric density variations are parameterized in the POD force model in terms of measurements of the flux of solar radiation at a wavelength of 10.7 cm and an index of the planetary geomagnetic activity that is excited by the interaction between the solar wind and the Earth's magnetic field. The solar flux index (Figure 5*a*) shows a secular increase over the 2-year period very similar to that of the bow tie maxima. Both time series increase by about a factor of 3 from late 1986 to late 1988. It thus appears that the general increase in the magnitudes of the orbit errors during the Exact Repeat Mission can be attributed to the increasing solar activity. The most recent 11-year sunspot cycle, which was one of the most active ever recorded [*Gorney*, 1990], began increasing from a minimum in October 1986 (coincident with the beginning of the Geosat data analyzed here) toward a maximum in late 1990. The shorter-period fluctuations in the bow tie maxima superimposed on the underlying trend are not well correlated with short-period variations in the solar flux index. Nor are they well correlated with the index of geomagnetic activity (not shown).

The generally poor relationships between the short-period variations in bow tie amplitudes and the indices of solar and geomagnetic activity are perhaps not surprising. As these indices form the basis for the atmospheric density estimates in the POD force model, any mismodeled short-period variations in density that would give rise to large bow tie amplitudes would not necessarily be highly correlated with either index. Moreover, the amplitudes of the bow tie patterns depend strongly on the quality and distribution of tracking data over each POD orbit arc. One of the primary objectives of the least squares adjustments of the orbit estimates to the tracking data in the POD procedure is to mitigate the effects of mismodeled short-period variations in atmospheric density.

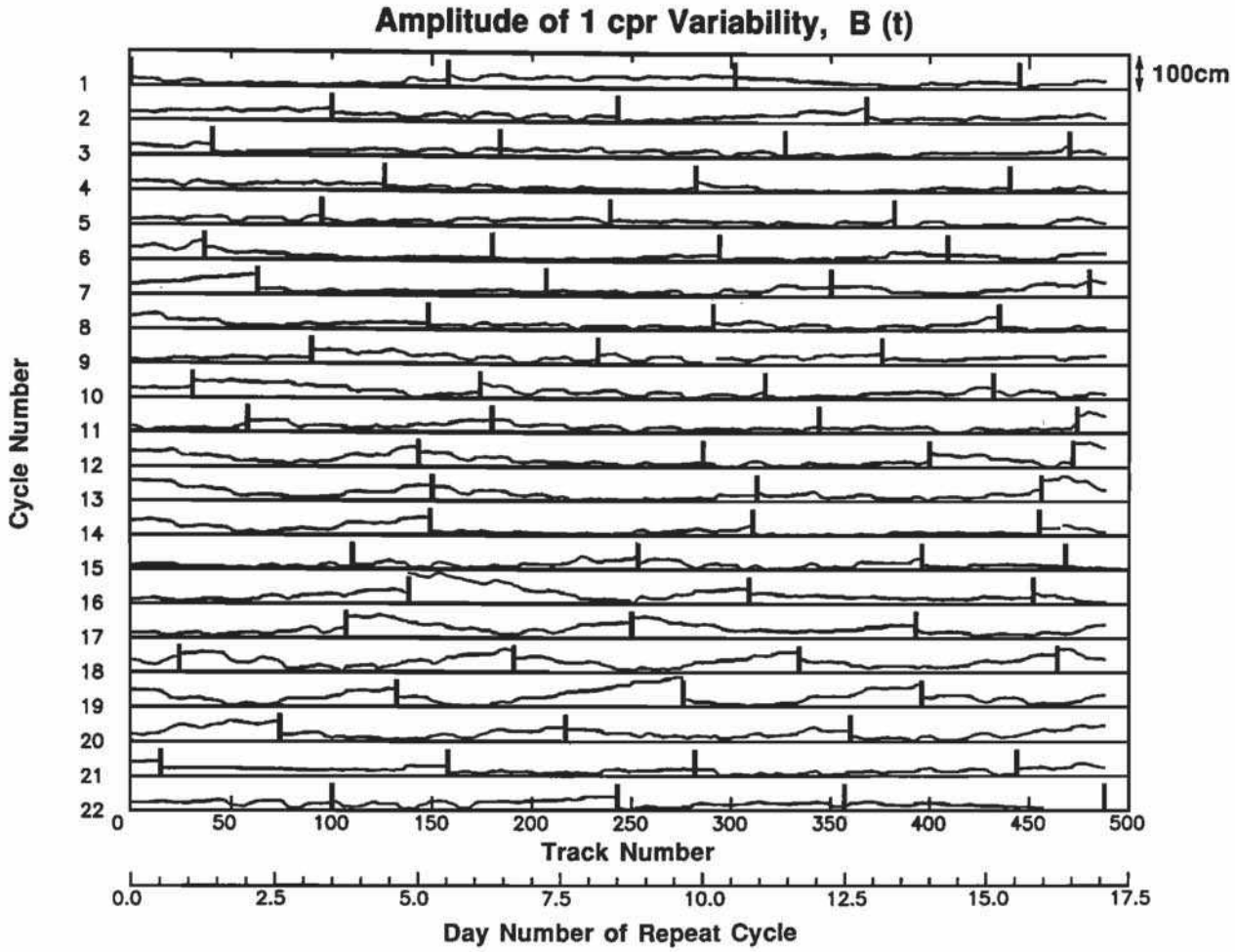

Fig. 3*a*. Time series of the amplitudes $B(t)$ of the 1-cpr GEM-T2 orbit errors (see equation (8)) from the first year of the Geosat 17-day Exact Repeat Mission, computed as described in the text with a span of 4.5 orbits. The vertical scale in centimeters is shown in the top right corner of the figure. The heavy vertical bars correspond to the times of orbit arc boundaries used in the GEM-T2 precision orbit determination.

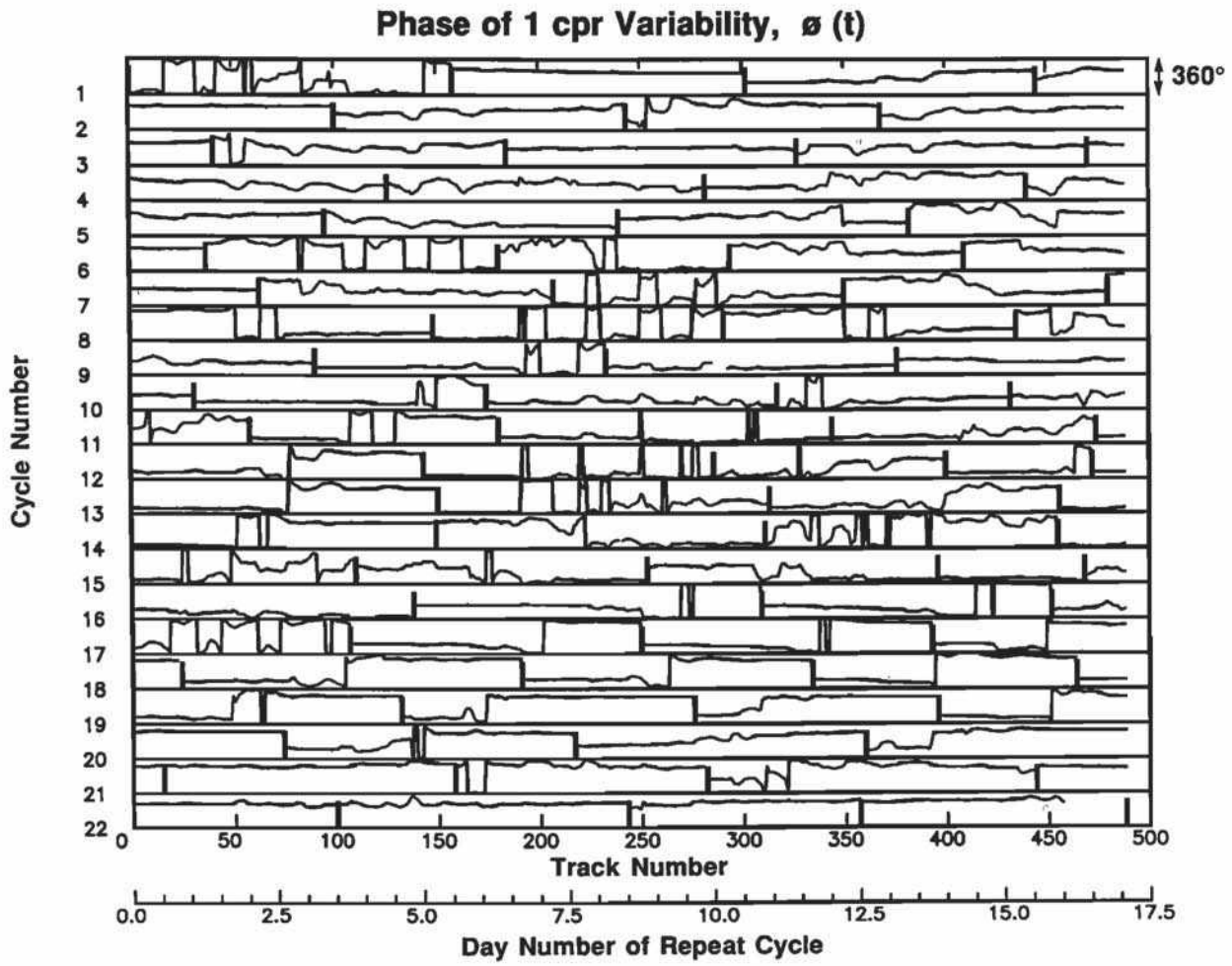

Fig. 3*b*. Time series of the phases $\phi(t)$ of the 1-cpr GEM-T2 orbit error (see equation (8)) with amplitudes shown in Figure 3*a*. The vertical scale in degrees is shown in the top right corner of the figure.

4.2. *Daily Modulations*

A more subtle, but perhaps more interesting feature of Figure 3*a* is a quasi-periodic variation of the orbit error sinusoid amplitude within many of the POD orbit arcs in the GEM-T2 data. This feature is more apparent in the example shown on an expanded vertical scale in Figure 6. This particular segment of data corresponds to the bow tie example in Figure 4*a*. The dashed line represents a smoothed fit to the time series of sinusoid amplitudes $B(t)$ and can be considered a measure of the bow tie effect discussed in section 4.1. The deviations of the orbit error sinusoid amplitude from the dashed line are the quasi-periodic orbit errors that are addressed in this section.

A smoothed fit to the sinusoid amplitudes like the dashed line in Figure 6 was computed for each POD orbit arc in the 2 years of Geosat data considered here. The quasi-periodic orbit errors are readily apparent in the time series of deviations from the smooth fits shown in Figure 7 for the first year of the Geosat Exact Repeat Mission. Visually, the periodicity of these features is about 1 day. The daily maximum values of the high-pass-filtered $B(t)$ are shown in Figure 5*c* for the full 2 years of data. Typical peak-to-peak ranges (which are a more relevant measure of the effects of the daily signals than the amplitude or rms variability) are about 14 cm, but peak-to-peak ranges of 25 cm or more (e.g., for the case shown in Figure 6) are common.

The time scales of the short period variations in orbit error in Figure 7 are quantified by the spectra in Figure 8 constructed separately from repeat cycles 1–19 and 20–38. (The behavior of the orbit error parameters was somewhat spurious after cycle 38 (see Figure 5), so these data were not included in the spectra in Figure 8.) Clearly defined spectral peaks occur at frequencies of 1 cpd and its first six harmonics. There are suggestions of additional spectral peaks at higher frequencies, but the energy levels are too low to be statistically significant. The rms variabilities within each of the spectral peaks are listed in Table 1. For both periods of data, the variability at these seven frequencies accounts for about one half of the total variance, about 75% of which is accounted for by the variability at 1 cpd alone. It must be kept in mind that the rms values in Table 1 are an average over each 19-cycle period of data; the amplitudes of short period variations in orbit error can be larger by a factor of 3 or 4 in some orbit arcs.

The m-daily variations in $B(t)$ represent short-period modulations of the bow tie patterns of 1-cpr sinusoid orbit error amplitudes. To see how these modulations impact the total orbit error, consider a track for which the contribution

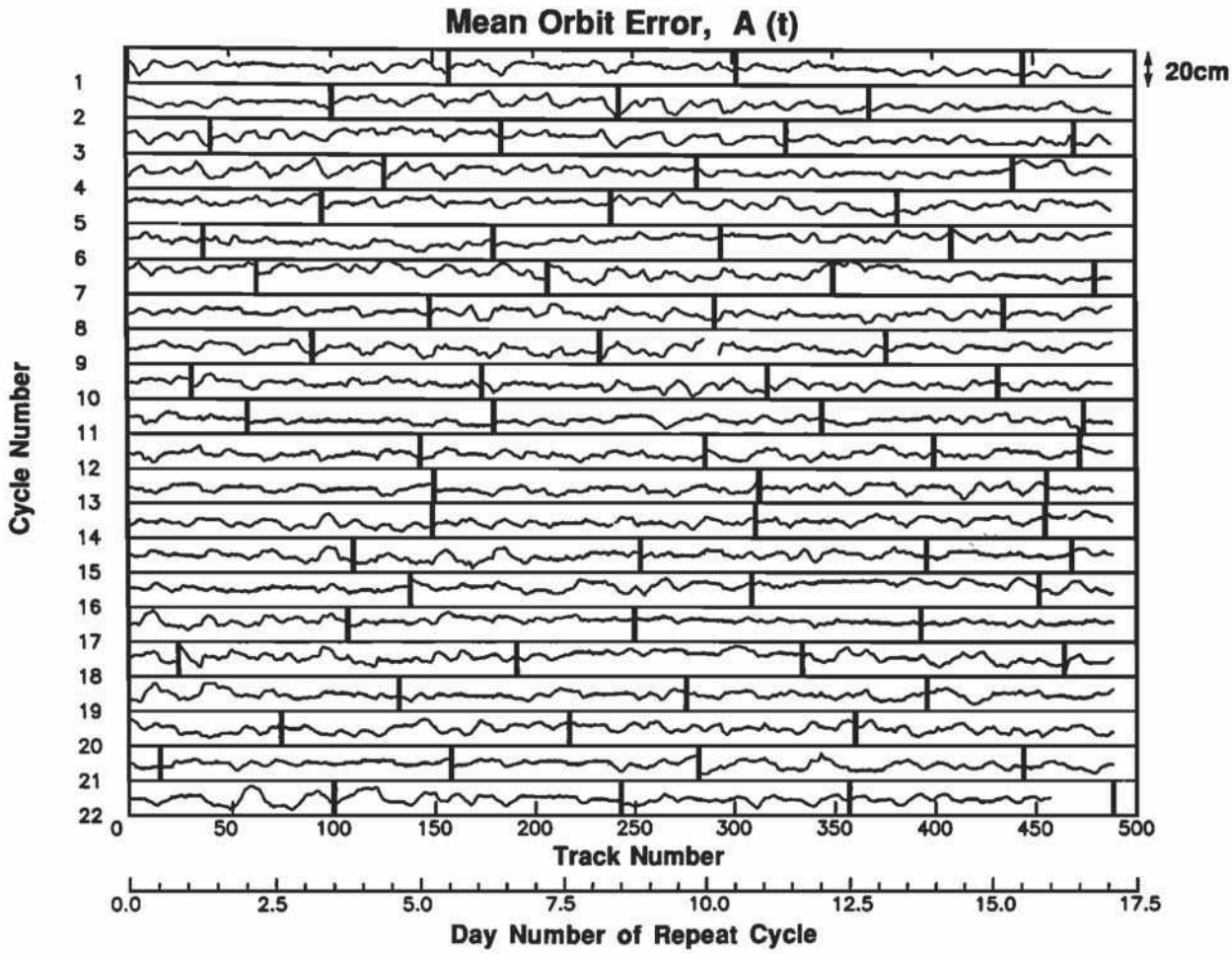

Fig. 3c. The same as Figure 3*a*, except of the mean GEM-T2 orbit errors $A(t)$ (see equation (8)).

to $B(t)$ from the spectral peak at m cpd has amplitude b_m and phase ϕ_m. The corresponding contribution to the total orbit error (8) can be written as

$$e'_m(t) = A(t) + b_m \cos\left[\frac{2\pi m t}{T_1} + \phi_m\right] \sin\left[\frac{2\pi t}{T} + \phi\right], \quad (9)$$

where T_1 is 1 day in the same time units as the orbital period T. Using the double angle formula, this can be expressed as

$$e'_m(t) = A(t) + \frac{b_m}{2}\left[\sin\left(2\pi f_m^+ t + \Phi_m^+\right) + \sin\left(2\pi f_m^- t + \Phi_m^-\right)\right], \quad (10)$$

where $f_m^{\pm} = \left(T^{-1} \pm m T_1^{-1}\right)$ and $\Phi_m^{\pm} = (\phi \pm \phi_m)$. The m-cpd modulations of $B(t)$ thus manifest themselves as spectral energy at the sum and difference frequencies f_m^+ and f_m^- separated from the fundamental 1-cpr frequency by $\pm m$ cpd, i.e., as split peaks on the shoulders of the dominant 1-cpr peak in the spectrum of orbit errors. The 1-cpd modulation frequencies are clearly evident and have been labeled in Figure 1*a*. The energy levels of the higher-harmonic m-cpd modulation frequencies are too small to be distinguished from the background noise for the degrees of freedom of the spectral estimates in Figure 1*a*, although they are clearly evident in the spectra of high-pass-filtered $B(t)$ in Figure 8.

The existence of the spectral peaks in Figure 8 at 1 cpd and its higher harmonics can be rationalized on a simple physical basis. Because more than 75% of the spectral energy in the figure is accounted for by the variability at 1 cpd, the short-period modulations of the bow tie patterns can be characterized to first order as simple sinusoidal variations with periods of 1 day. The spectral energies at the higher-harmonic m-cpd frequencies are necessary to account for the fact that the underlying daily modulations are not purely sinusoidal (see Figure 9). The detailed shapes of these "mini bow tie" patterns vary for each POD orbit arc and from one day to another within a given orbit arc, depending on the quality and distribution of tracking data available and on the magnitude of the highly variable time-dependent drag errors that arise because of mismodeled variations in atmospheric density at the altitude of the satellite.

Isolating the source of the daily modulations of 1-cpr orbit error is more speculative than demonstrating their existence. An attempt is made here to offer what we believe to be the most likely explanation; confirmation of this hypothesis would likely require POD simulations, which are beyond the scope of this paper. Actual oceanographic variability can be ruled out as highly unlikely; it would be difficult to conceive of a dynamical explanation for such spatially and temporally coherent sea level variations over the complex sampling pattern mapped out along

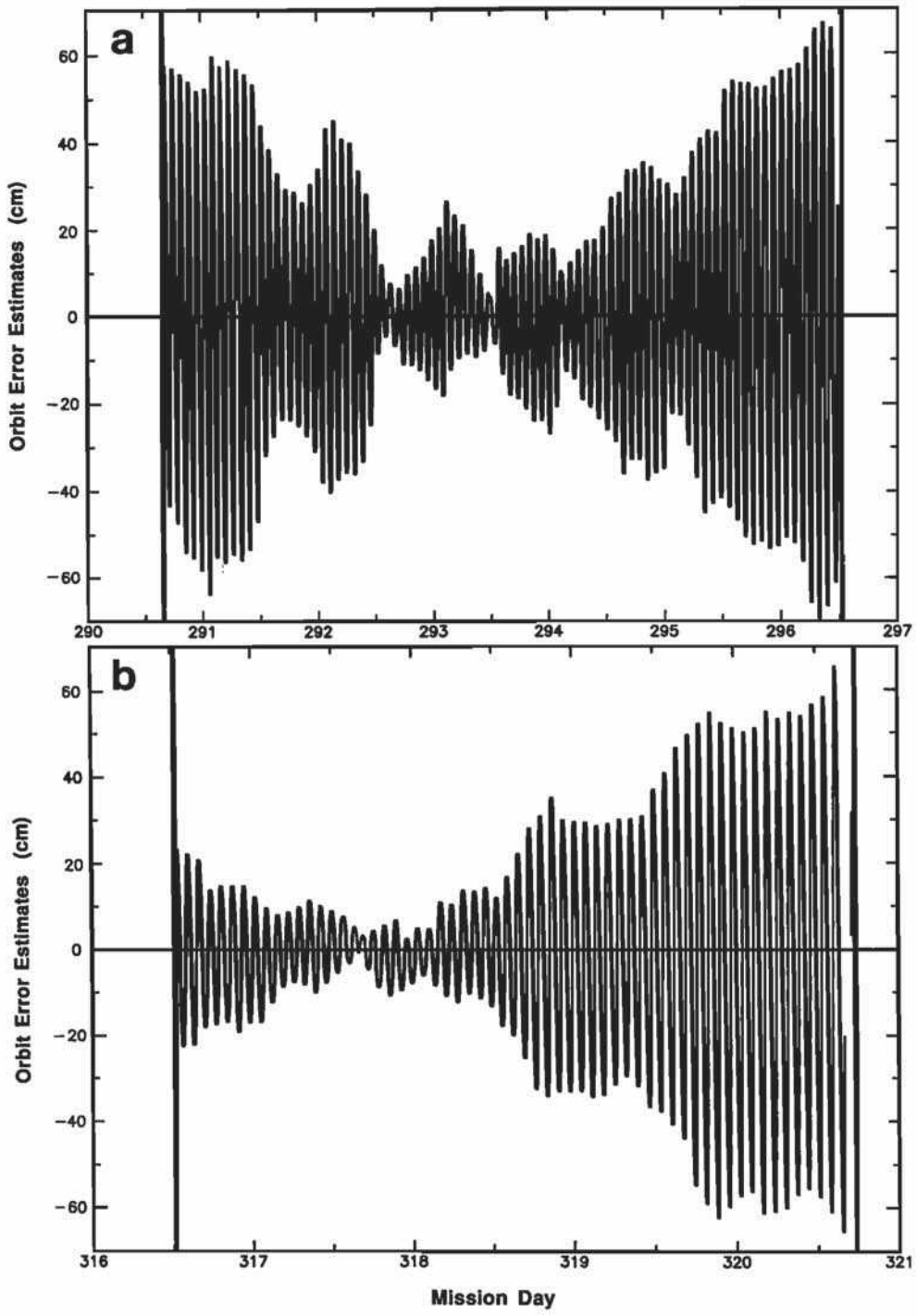

Fig. 4. Time series of the orbit error estimates for (*a*) the first complete orbit arc of repeat cycle 18 beginning at approximately day 0.8 of the 17-day repeat period, and (*b*) the second complete orbit arc of repeat cycle 19 beginning at approximately day 7.5 of the 17-day repeat period. The "knot" of the bow tie pattern is near the middle of the orbit arc in case Figure 4*a* but is closer to the beginning of the orbit arc in Figure 4*b*.

the satellite ground track. It also seems unlikely that mismodeled ocean or solid earth tides could result in such coherent variability at 1 cpd and its first six harmonics as sampled along the satellite ground track. Other possible explanations for quasi-periodic modulations of the 1-cpr orbit error that cannot be definitively rejected are range measurement errors from mismodeled ionospheric or tropospheric effects on atmospheric refraction. However, atmospheric correction errors of the magnitude and spatial scale necessary to account for the larger of the mini bow ties observed (25 cm peak-to-peak or more) seem very unlikely. Mismodeled tidal forces on the satellite have no significant daily perturbations. Mismodeled tidal forces on atmospheric density at the altitude of the satellite also seems an unlikely explanation.

The so-called "*m*-daily orbit perturbations" that arise

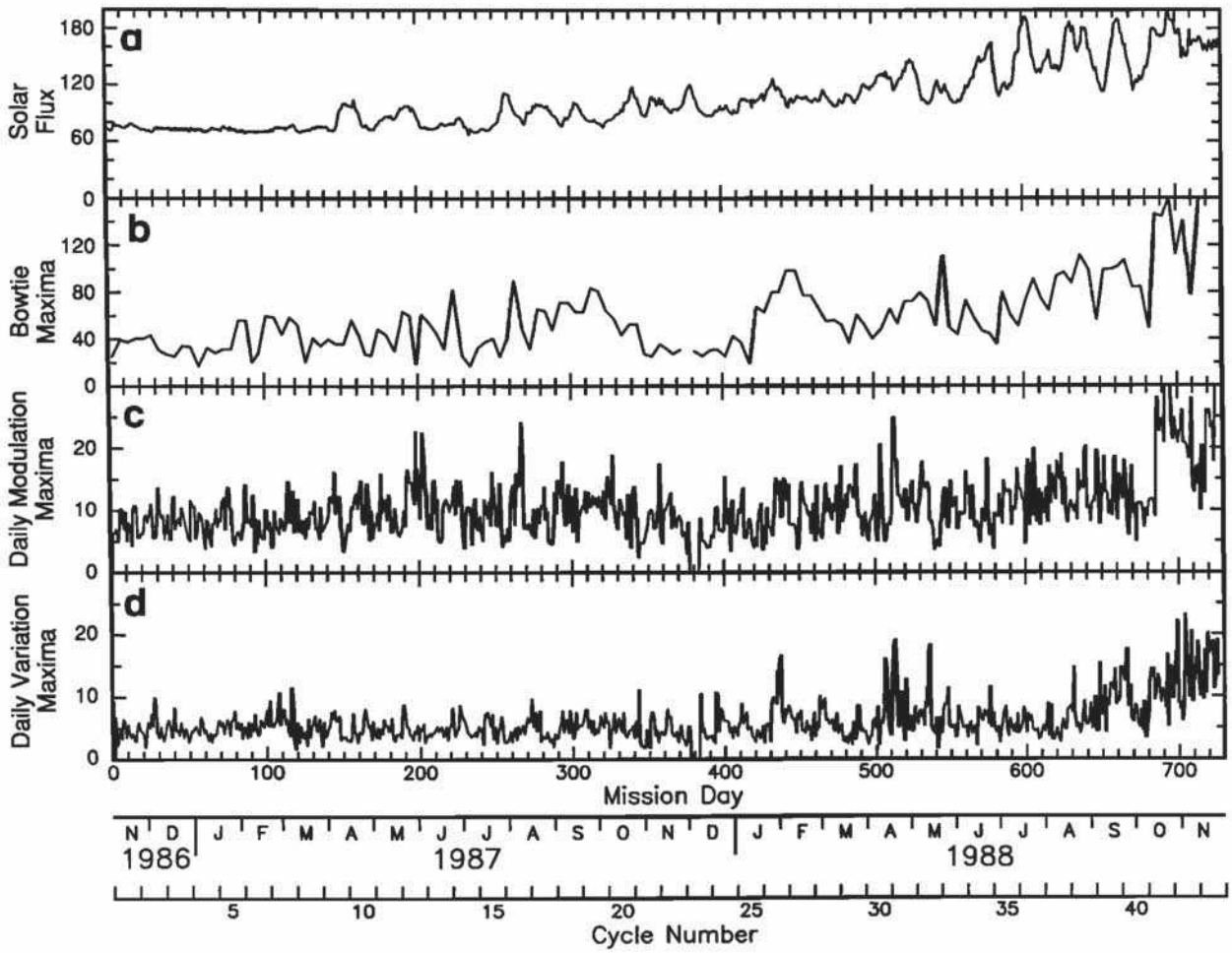

Fig. 5. Time series for the first 2 years of the Geosat Exact Repeat Mission of (*a*) the solar flux at 10.7-cm wavelength, (*b*) the maximum bow tie amplitudes of $B(t)$ (see section 4.1) for each 5- to 6-day POD orbit arc, (*c*) the daily maximum mini bow tie amplitudes (approximately half of the peak-to-peak range of the daily modulation) of high-pass filtered $B(t)$ (see section 4.2), and (*d*) the daily maximum magnitude (approximately half of the peak-to-peak range of the daily variations) of the constant offset term $A(t)$ (see section 4.3).

because of uncertainties in the Earth's gravity field may seem a plausible explanation for the daily modulations. This effect, which has long been well known within the POD community [e.g., *Marsh and Williamson*, 1980; *Wagner*, 1985], can be described heuristically as follows. The order m of a particular term in a spherical harmonic expansion of the gravity field describes the number of longitudinal (east-west) perturbations relative to a spherically symmetric gravity field. Ignoring the small precession rate of altimetric satellites (less than 3° per day), the plane of the satellite orbit is fixed in an inertial reference system. As a result of the rotation of the Earth, any uncertainty in an order m coefficient in the spherical harmonic expansion of the gravity field introduces m mismodeled perturbations on the satellite orbit during a 24-hour period. Such gravity errors would thus result in an m-cpd modulation of the predominantly 1-cpr orbit error.

The m-daily perturbations in the satellite orbit from uncertainties in any of the order 1 through 7 geopotential coefficients would result in a spectrum similar to that shown in Figure 8. However, an important feature that distinguishes the effects of m-daily gravity errors from other sources of periodic variations in orbit error is that these static components of gravity effects are exactly repeatable during every cycle of an exact repeat orbit (neglecting the relatively minor complicating effects of cross-track variations in the satellite ground track [*Brenner et al.*, 1990] and the low-frequency effects of precession of the argument of perigee). The m-daily periodic modulations of orbit error of gravitational origin are thus part of the time-invariant orbit error discussed in section 2. In the simultaneous solution method used here to estimate orbit error, these effects have been removed as part of the mean sea level $\bar{h}(x_j)$ estimated simultaneously with the time-dependent orbit errors $e_i'(x_j)$. Inspection of Figure 7 verifies that this is indeed the case. While there are examples of phase-locked orbit error modulations with similar shapes and amplitudes at the same point in different cycles of the 17-day repeat period, there are many more examples of incoherent modulations between different repeat cycles. There are also cases where the daily modulations are similar in amplitude and shape but 180° out of phase at the same point in different repeat cycles. The m-cpd modulations of the amplitude of 1-cpr sinusoid orbit error clearly cannot be of gravitational origin.

Consideration of the details of the POD technique used

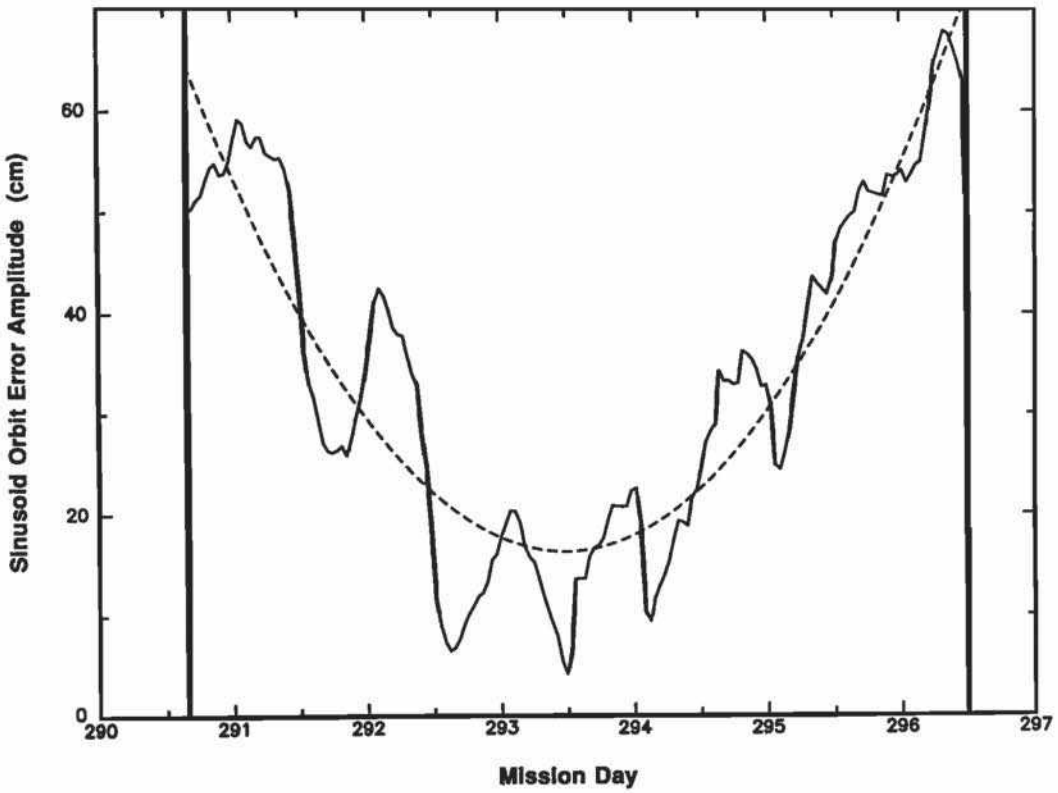

Fig. 6. An expanded plot of the amplitudes of the 1-cpr orbit error estimates shown in Figure 3*a* for the first complete orbit arc of repeat cycle 18 (the same time period as the orbit error estimates shown in Figure 4*a*). The heavy vertical bars correspond to the times of the orbit arc boundaries and the dashed line represents a smoothed fit to the sinusoid orbit error amplitudes.

to generate the GEM-T2 data suggests an explanation that we believe to be the most likely source of the daily modulations of orbit error amplitude. As is summarized in Appendix B, a drag scaling parameter in the force model used in the POD was adjusted over each daily interval beginning at 0000 UT to compensate for errors in the force model and uncertainties in atmospheric density at the altitude of the satellite. This adjustment was achieved by including step function changes in the drag scaling parameter for each 24-hour period in the state vector updated once for each POD orbit arc on the basis of a least squares fit of the predicted orbits to ground-based satellite tracking measurements acquired during the 5- to 6-day orbit arc.

The relationship between the magnitude of the daily modulation of orbit errors and the timing of the least squares adjustment of drag coefficient can be investigated from Figure 9. Although the daily modulations cannot be characterized simply, these examples suggest that there may be a tendency for the amplitudes of the daily modulations to be smallest near 0000 and 1200 UT and largest near 0600 and 1800 UT. (The example from cycle 22, which is phase shifted by about 90° from the other examples, is a notable exception.) This interpretation implies that the knots of the mini bow ties tend to occur near the times of the daily least squares adjustments and about 12 hours later, resulting in a quasi-sinusoidal modulation of orbit errors.

An attempt to relate the amplitudes of the daily modulations to solar activity was only modestly successful (Figure 5*c*). The weak secular increase in the maximum amplitude of each daily mini bow tie over the 2-year period may be related to the threefold increase in solar flux over the same period. However, the shorter-period fluctuations in the daily mini bow tie amplitudes are uncorrelated with short-period variations in either the 10.7-cm solar flux (Figure 5*a*) or the index of geomagnetic activity discussed previously. The slight increase in the frequency of occurrence of large-amplitude daily modulations (Figure 5*c*) and a 50% increase in the variance of the high-pass-filtered $B(t)$ (Table 1) during the second year of data suggest that the increased solar activity may have had some influence on the daily modulation of orbit errors, but the effect was not strong. This result is perhaps not surprising. Mismodeled atmospheric density variations that would give rise to increased orbit error amplitudes would not necessarily be correlated with either of these two indices from which density is parameterized in the POD force model. Most of the mismodeled atmospheric density variations probably have periods longer than a day and thus account for the long-period bow tie patterns discussed in section 4.1.

4.3. *Daily Variations*

The time series of the mean orbit error along each track (the constant offset term $A(t)$ in equation (8)) shown in Figure 3*c* is dominated by a quasi-periodic daily variability very similar to that of the high-pass-filtered $B(t)$ shown in Figure 7. The peak-to-peak ranges of these daily variations are typically 6 cm, which is about half the typical range of the daily modulations of 1-cpr orbit error discussed in section 4.2. During the first year of data shown in

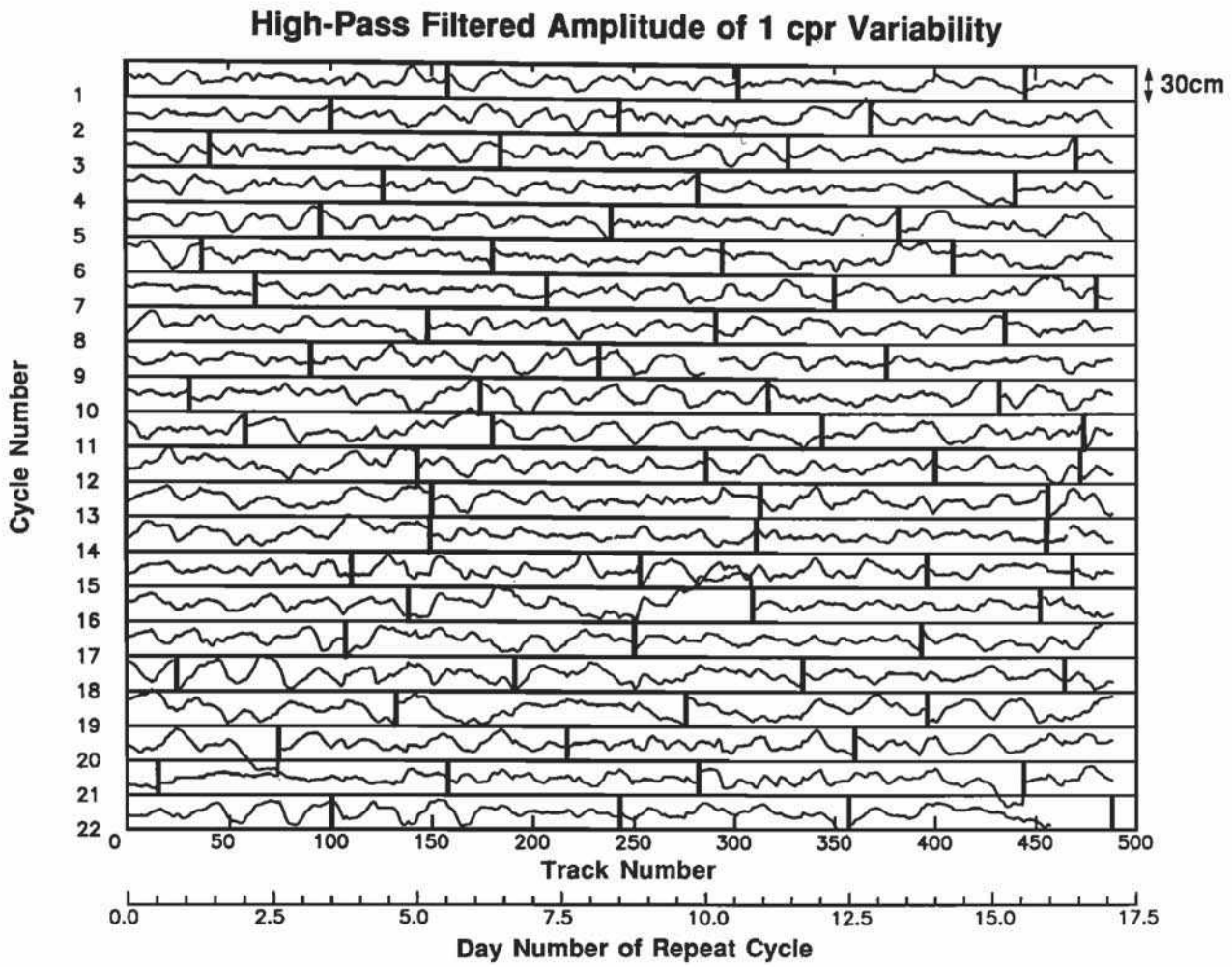

Fig. 7. Time series of high-pass-filtered amplitudes $B(t)$ (see equation (8)) of the 1-cpr orbit error estimates shown in Figure 3*a*. The high-frequency variations in the sinusoid orbit error amplitudes were isolated by removing a smoothed fit for each orbit arc like the example shown by the dashed line in Figure 6. The vertical scale in centimeters is shown in the top right corner of the figure.

Figure 3*c*, daily variations with range as large as 15 cm were experienced (e.g., during the early portion of cycle 22). Daily peak-to-peak ranges of this magnitude were common during the second year of the Exact Repeat Mission, with many occurrences of 25 cm and larger ranges (Figure 5*d*).

The spectra of these daily variations of the mean orbit error are shown in Figure 10 for repeat cycles 1–19 and 20–38. The characteristics of these spectra are very similar to those of the daily modulations shown in Figure 8. Clearly defined spectral peaks are evident at the same seven frequencies (1 cpd and its first six harmonics). The rms variabilities within each of these spectral peaks are listed in Table 2. As with the daily modulations, the variability at these seven frequencies accounts for about half of the total variability of $A(t)$, most of which is accounted for by the variability at 1 cpd alone. To first order, the underlying shapes of these low-frequency variations in orbit error are thus sinusoidal with a period of 1 day. The energy at the higher harmonics accounts for the fact that the daily variations are not purely sinusoidal.

It should be clear, but is perhaps worth emphasizing, that these daily variations in the orbit errors are fundamentally different from the daily modulations of 1-cpr orbit error discussed in section 4.2. The daily variations addressed in this section are independent of the dominant 1-cpr orbit error. They represent mismodeled daily variations in the mean semimajor axis of the satellite orbit. Consequently, they show up as separate spectral peaks (rather than split peaks centered on the 1-cpr spectral peak) in the spectrum of orbit errors. The 1- and 2-cpd spectral peaks are clearly evident and have been labeled in Figure 1*a*. The energy levels of the higher-harmonic m-cpd variations are too small to be seen convincingly for the degrees of freedom of the spectral estimates in Figure 1*a*, although they are clearly evident in the spectra of $A(t)$ in Figure 10.

Because the daily variations of orbit error are so similar in character to the daily modulations of 1-cpr orbit error, the causes are very likely the same. In section 4.2, we have presented what we feel is a convincing case that these daily signals in the orbit errors arise because of the daily least squares adjustment of the drag coefficients in the POD used to generate the GEM-T2 orbits. Large-amplitude daily variations in orbit error were much more commonplace (Figure 5*d*) and the overall variance of $A(t)$ was more than a factor of 2 larger (Table 2) during the second year of data. This increase in low-frequency orbit errors is probably

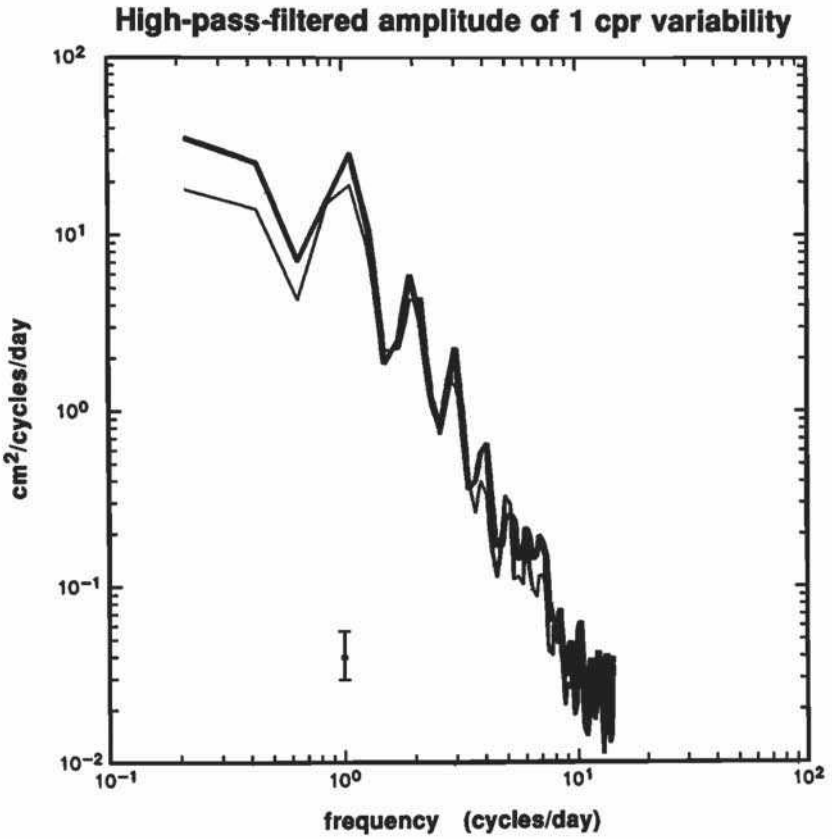

Fig. 8. Power spectral density of the high-pass-filtered amplitudes $B(t)$ (see equation (8)) of the 1-cpr orbit error estimates for repeat cycles 1–19 (thin line) and 20–38 (thick line). The individual spectra with 2 degrees of freedom for each of the orbit arcs of duration 4.6 days or longer were ensemble averaged to obtain a total of approximately 76 degrees of freedom. The error bars represent 95% confidence intervals.

TABLE 1. The rms Variability and Percentage of Total Variance of the High-Pass Filtered $B(t)$ in Equation (8) Within Each of the Dominant Spectral Peaks in Figure 8, the Root Sum of Squares (rss) Total at These Frequencies, and the Total rms Over All Frequencies for Cycles 1–19 (November 1986 to October 1987) and Cycles 20–38 (October 1987 to September 1988) of the Geosat Exact Repeat Mission

	Cycles 1–19		Cycles 20–38	
Frequency, cpd	rms, cm	Variance, %	rms, cm	Variance, %
1	2.98	40.5	3.42	36.6
2	1.35	8.4	1.40	6.1
3	0.91	3.8	0.89	2.5
4	0.40	0.7	0.50	0.8
5	0.37	0.6	0.40	0.5
6	0.25	0.3	0.31	0.3
7	0.22	0.2	0.28	0.2
rss	3.45	54.6	3.88	47.0
Total	4.67	100.0	5.66	100.0

The rss corresponds approximately to one third of the typical peak-to-peak range of the daily modulations.

related to mismodeled atmospheric density variations from the increased solar flux over the 2-year period (Figure 5*a*).

5. GEM-T2 Versus NAG Residual Height Data

The importance of POD accuracy for altimetric studies of time-dependent sea level variability has long been an unresolved issue. The availability of the GEM-T2 and NAG data sets, which differ by an order of magnitude in orbit accuracy, offers an excellent opportunity to address this issue. Common wisdom has it that the crude accuracy of the NAG orbits, after suitable orbit error estimation and removal, is acceptable for studies of time-dependent mesoscale variability but severely limits applications for studies of large-scale variability. The validity of this notion depends on the spectral characteristics of the orbit error, and not just the magnitude of the orbit error. On the basis of the estimated spectrum in Figure 1*b*, the time-dependent NAG orbit errors appear to be almost totally 1 cpr. Most of this orbit error should be removed by the simultaneous solution method described in section 3, in which case the residual height data would be of comparable quality to the residual height data obtained from the much more accurate GEM-T2 orbits.

To investigate this hypothesis, the simultaneous solution method was applied to the NAG data using the same 4.5-orbit span applied in section 4 to the GEM-T2 data. The NAG and GEM-T2 residual height data $h_i'(x_j)$ (see equation (1)), after the respective mean sea level and time-dependent orbit error estimates were removed, were then compared in a variety of ways. A traditional, although not comprehensive, measure of the quality of orbit error corrections is the rms difference between height estimates from ascending and descending ground tracks at crossover points. The obvious flaw in the logic of this quality metric is that it implies that an rms crossover

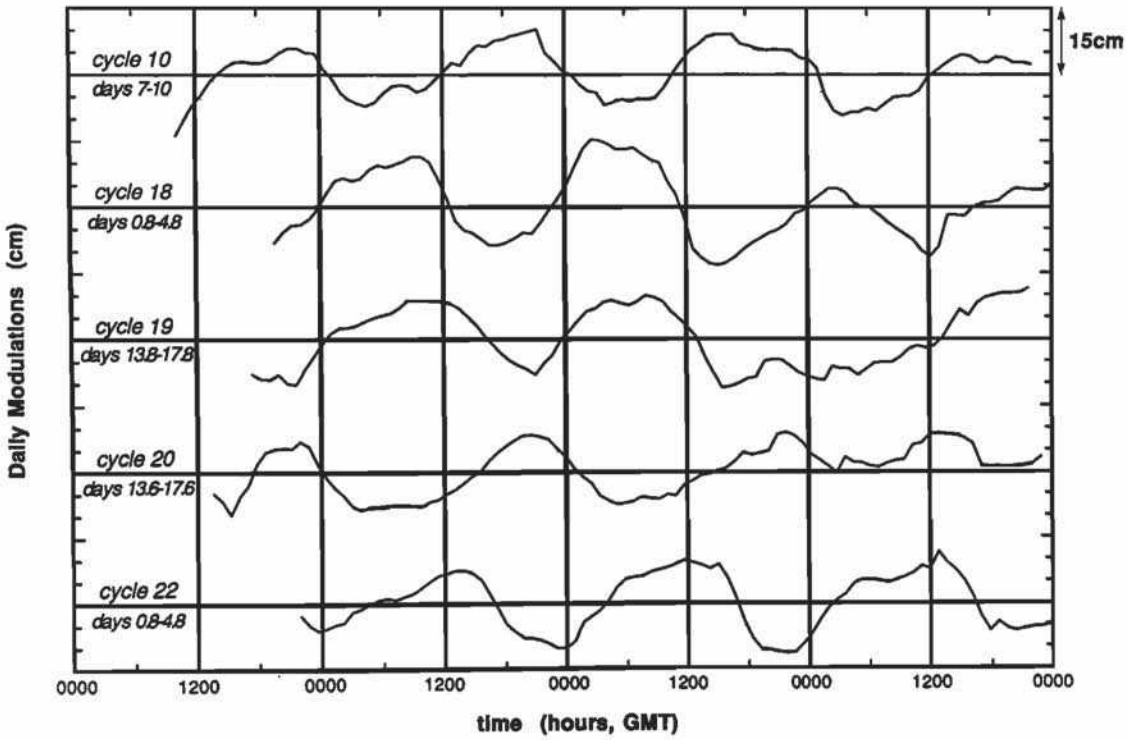

Fig. 9. Expanded plots of the high-pass-filtered amplitudes of 1-cpr orbit error estimates shown in Figure 7 for segments of data from (top to bottom) repeat cycles 10, 18, 19, 20, and 22. The vertical scale in centimeters is shown in the top right corner of the figure.

difference of zero would represent the best possible orbit error correction. In fact, such a result would indicate that all of the oceanographic signal was removed along with the orbit error, which is clearly undesirable. Crossover difference results must therefore be considered only a qualitative measure of the effectiveness of a given orbit error estimation scheme. The averages of the rms crossover differences computed globally for each of the first 22 repeat cycles were 13.2 and 13.3 cm, respectively, for the GEM-T2 and NAG residual height data. By this measure, then, the much higher quality GEM-T2 data do not appear to be significantly different from the NAG data after removing the mean sea levels and time-dependent orbit errors by the simultaneous solution method described in section 3. A similar conclusion has been reached by *Rosborough and Marshall* [1990].

Pointwise comparisons offer a much more quantitative assessment of the similarity between the GEM-T2 and NAG residual height data. For this purpose, regression statistics were computed for each pass (half orbit) of data during the first year of the Geosat Exact Repeat Mission. A simple linear regression between the two data sets resulted in a mean of 1.0 and a small standard deviation of 0.04 for the slope estimated for each pass and a mean of 0.0 cm and relatively large standard deviation of 2.2 cm for the constant term. The cross correlations between the GEM-T2 and NAG residuals were greater than 0.99 for more than 90% of all passes. A histogram of rms differences computed for each pass resembled a Rayleigh distribution with an average rms difference of 1.4 cm and a peak in the distribution at 0.8 cm. Much of the rms difference can be attributed to relative biases for each pass, as is evident from the large scatter of the constant term in the regression statistics. When the mean difference for each pass is removed, the average rms difference is reduced to 0.9 cm and the peak in the distribution shifts to 0.5 cm. In consideration of the fact that the original GEM-T2 and NAG data analyzed here were stored on disk with a coarse resolution of 1 cm, the level of agreement between the two residual height data sets after removing the mean sea level and time-dependent orbit error estimates is quite impressive.

The spectral characteristics of the differences between GEM-T2 and NAG residual heights were quantified from analysis of 11 repeat passes of a 14,000-km ascending track across the central Pacific. The squared coherences were greater than 0.99 and the phase differences were not statistically different from zero at all wavenumbers. The spectra of the residual heights and the differences between the GEM-T2 and NAG residual heights are shown in Figure 11. At wavelengths shorter than 1000 km, the difference spectrum is characterized by an approximate white noise floor. At longer scales, the spectral energy increases abruptly by more than an order of magnitude. The predominantly long-wavelength character of the differences explains the previously noted improvement in the rms difference statistics when the mean difference is removed from each pass of data; to first order, the long-wavelength differences can be approximated by a relative bias along each pass. The differences between the GEM-T2 and NAG residual heights at low wavenumbers probably arise from statistical instabilities of the least squares estimates of the parameters a_i, b_i, and c_i in (2), rather than from peculiar behavior of the less accurate NAG orbits.

For these 11 passes of this particular track, the total rms variability of the differences between the GEM-T2

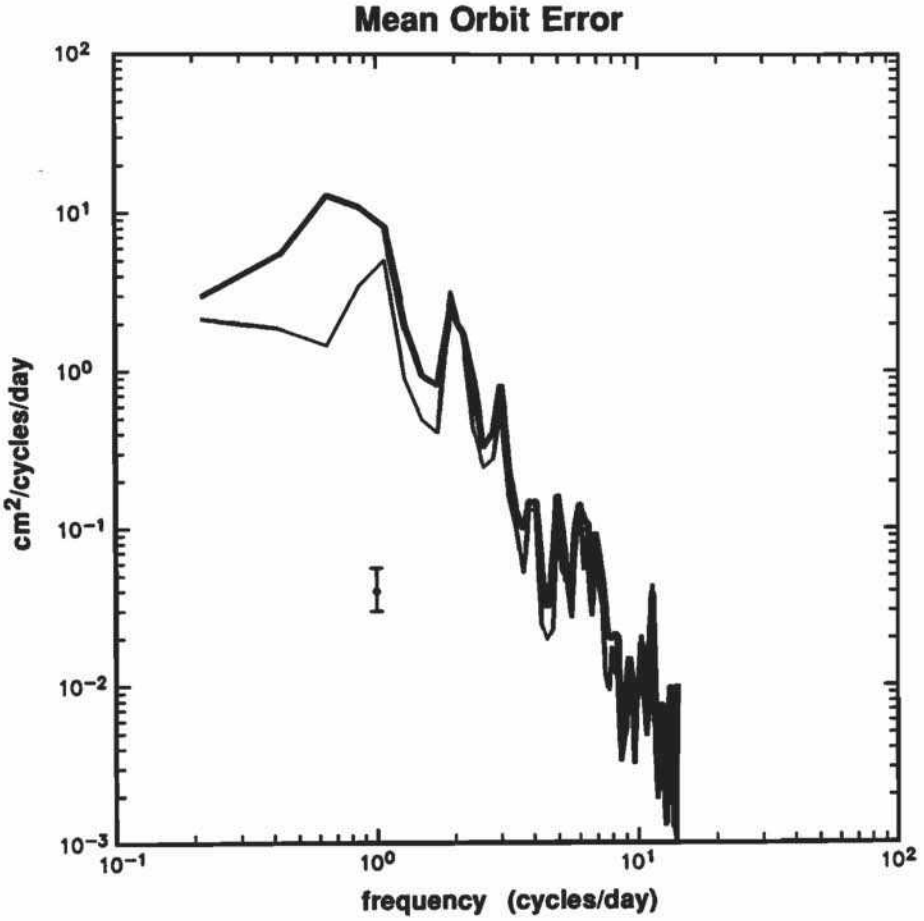

Fig. 10. Power spectral density of the mean orbit errors $A(t)$ (see equation (8)) for repeat cycles 1–19 (thin line) and 20–38 (thick line). The degrees of freedom and confidence intervals are the same as in Figure 8.

TABLE 2. The Same as Table 1, Except of $A(t)$ in Equation (8) From the Spectrum Shown in Figure 10

	Cycles 1–19		Cycles 20–38	
Frequency, cpd	rms, cm	Variance, %	rms, cm	Variance, %
1	1.36	35.8	2.03	35.9
2	0.94	17.1	0.95	7.9
3	0.36	2.5	0.42	1.5
4	0.24	1.1	0.25	0.6
5	0.16	0.5	0.19	0.3
6	0.18	0.6	0.32	0.9
7	0.15	0.4	0.19	0.3
rss	1.73	58.1	2.33	47.4
total	2.27	100.0	3.39	100.0

The rss corresponds approximately to one third of the typical peak-to-peak range of the daily variations.

and NAG residual heights over wavelengths longer than 1000 km is only 0.35 cm, accounting for about one fourth of the total variance of the differences. This long-wavelength energy of the differences is smaller than the time-dependent ocean signal over the same length scales (see top curve in Figure 11) by 2 orders of magnitude and is therefore of little consequence for this track. This may not always be the case, however. The spectral energy of the differences between NAG and GEM-T2 residual data is always dominated by variability at wavelengths longer than 1000 km. For some passes, the variance of the long-wavelength differences may be more comparable to that of the long-wavelength, time-dependent ocean signal than for the case shown in Figure 11.

It can be concluded from this analysis that, although the accuracy of POD is of utmost importance to altimetric studies of time-invariant sea level, it is not important to time-dependent studies of mesoscale variability from collinear data, provided that a long-arc (several orbital periods) orbit error estimation technique such as that applied here is used. This of course assumes that the time-dependent orbit error is predominantly 1 cpr, as it apparently is in both the GEM-T2 and NAG data (Figure 1). For studies of large-scale variability (wavelengths longer than 1000 km), the accuracy of the POD becomes more of a concern.

It should be noted that POD accuracy can be important for time-dependent studies on all length scales when the orbit errors are estimated by the traditional low-order polynomial approximations over arc lengths of 1000–3000 km. Residual errors in such polynomial approximations will be smaller for more accurate POD, thus resulting in more accurate data for time-dependent sea level studies [*Cheney et al.*, 1991].

6. Summary and Discussion

The spectral characteristics of Geosat time-dependent orbit errors have been examined in detail for altimeter data

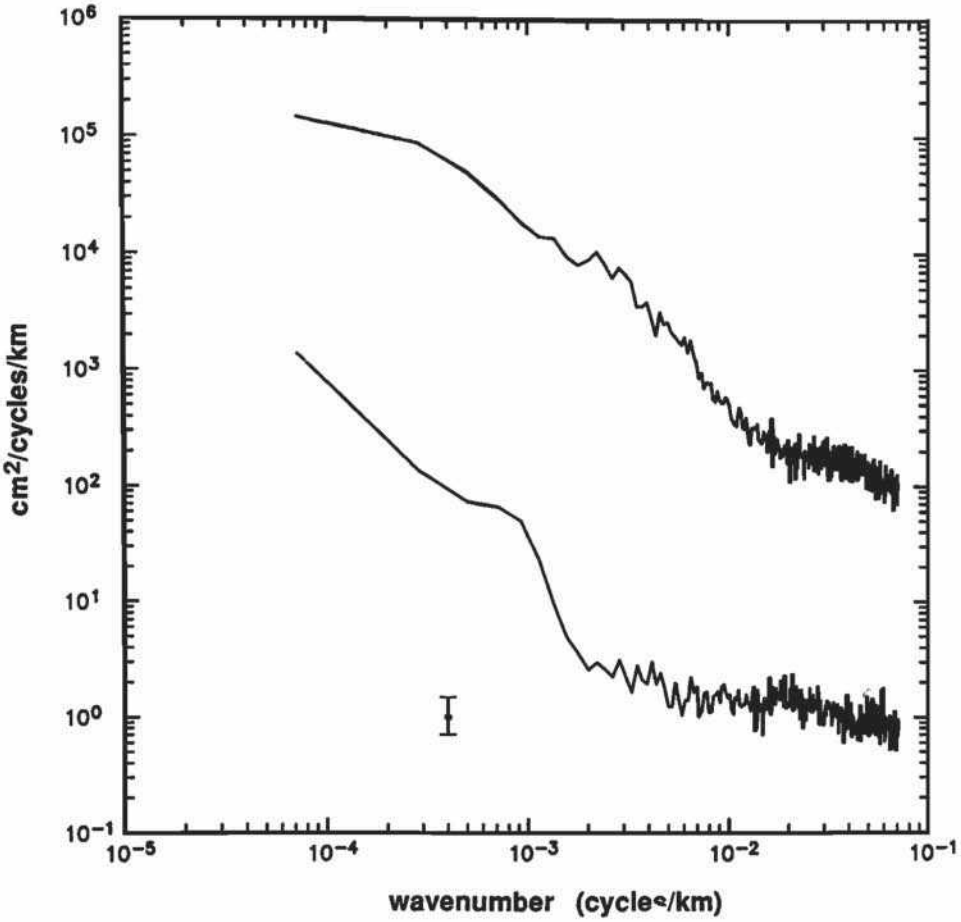

Fig. 11. Power spectral densities of the residual height data (top curve) for the GEM-T2 and NAG data sets (indistinguishable on this plotting scale) along a 14,000 km ascending ground track across the central Pacific. The power spectral density of the differences between the GEM-T2 and NAG residual height estimates is shown by the bottom curve. The individual spectra with 2 degrees of freedom for each of 11 repeats of the ground track were ensemble averaged and then band averaged to obtain a total of 66 degrees of freedom. The error bars represent the 95% confidence intervals.

from the GEM-T2 orbits, which are the most accurate of the widely used orbits presently available for Geosat. (There are other orbits available with reported improved accuracies, but these have not yet received widespread attention.) Although the total orbit error is very complex and difficult to estimate, the time-dependent component is almost totally characterized by narrow-band variability at the orbital period. The slowly varying amplitudes and phases of the 1-cpr orbit errors were estimated using a slightly modified version of the simultaneous solution method developed by *van Gysen et al.* [1992] for application to altimeter data from exact repeat orbit configurations. The method provides least squares estimates of mean sea level for each track (half orbit) of Geosat data and the amplitude and phase of 1-cpr orbit error for each repeat pass along the track. Low-frequency variations in orbit error (periods longer than several orbital periods) are accommodated within the orbit error estimation method by including a constant offset term in the least squares estimate for each repeat pass.

The orbit error estimates obtained by the simultaneous solution very successfully recover the well-known bow tie pattern in the orbit error amplitude over the period of each POD orbit arc in the GEM-T2 data. The bow tie effect is characterized by smallest amplitudes of 1-cpr orbit error near the middle of each POD arc and larger amplitudes (as large as 160 cm, corresponding to a 320-cm peak-to-peak range, in the 2 years of Geosat data considered here) at the ends of the arc. (The exact timing of the minimum and maximum depends on the distribution and quality of ground-based tracking data acquired during the orbit arc.) The bow tie characteristic arises because of the details of the GEM-T2 POD least squares adjustment of the satellite initial conditions and selected force model parameters performed every 5–6 days on the basis of ground-based tracking measurements. An empirical technique such as the simultaneous solution method used here is required to remove these orbit errors from altimeter height data.

A more detailed analysis found that the 1-cpr sinusoid orbit error amplitudes are modulated by daily variations at frequencies of 1 cpd and its first six harmonics. The 1-cpr spectral peak is therefore actually split into a series of peaks at frequencies of 1 cpr plus or minus m cpd, where m includes the integers between 1 and 7. The rms peak-to-peak range of the daily modulation of orbit errors is about 14 cm, but peak-to-peak ranges of 25 cm were common in the 2 years of data analyzed here, especially during the second year.

The analysis also identifies a daily variation in the mean orbit error at the same frequencies of 1 cpd and its higher harmonics. The rms peak-to-peak range of these mismodeled daily variations in the mean semimajor axis of the Geosat orbit is about half that of the daily modulations of 1-cpr orbit error, but peak-to-peak ranges of 25 cm were common toward the end of the 2-year data record.

The cause of the daily signals in the orbit error is not known for certain at present. A case has been made here that these daily signals are introduced by daily least squares adjustments of the drag coefficient in the POD force model used to generate the GEM-T2 orbits. The detailed shapes of the daily signals depend on the distribution of tracking data over the POD orbit arc and on the size and character of the drag error that the POD adjustment attempts to remove. To first order, the daily signals are sinusoidal with periods of 1 day. The smaller spectral energies at the higher harmonics of 1-cpd variability account for the fact that the daily signals are not purely sinusoidal. The existence of daily signals in the orbit errors is perhaps not surprising, since daily step function adjustments of the drag scaling parameters only partially mitigate the errors arising from uncertainties in atmospheric drag and air density at the altitude of the satellite.

Preliminary analysis of TOPEX/Poseidon data also shows evidence of daily signals in the orbit errors (S. Klosko, personal communication, 1993). These daily errors are evidently a robust characteristic of POD when errors in the modeling of atmospheric drag are corrected in some average sense over a specific time interval (24 hours in the Geosat GEM-T2 and TOPEX/Poseidon orbits).

An obvious question that arises from this analysis is whether the ~14-cm rms peak-to-peak ranges of the daily modulations of 1-cpr orbit error and the ~6-cm rms peak-to-peak daily variations of mean orbit error are large enough to be significant for oceanographic applications of Geosat data. If the interest is in energetic mesoscale variability on length scales shorter than ~1000 km, the orbit errors can be adequately removed by the bias and tilt or quadratic least squares fits used traditionally in altimetric studies. The daily modulations of orbit error are then of little consequence, since they appear constant over such short data arcs and are therefore removed as part of the constant parameter in the polynomial fits. For studies of larger-scale oceanographic variability, the form of the orbit error modeling becomes much more important; a weighted least squares fit to a 1-cpr sinusoid over long orbit arcs is far superior to polynomial fits. The noise from the daily signals is comparable to the magnitude of oceanographic variability over length scales longer than ~1000 km [*Chelton et al.*, 1990; *Wunsch*, 1991]. It is therefore important that this component of the time-dependent orbit error be removed by empirical techniques for large-scale oceanographic applications of altimeter data. The simultaneous solution method used here successfully resolves the daily signals and is therefore well suited for such purposes.

An important conclusion from this study is that altimetric studies of time-dependent mesoscale sea level variability (wavelengths shorter than about 1000 km) from collinear data are not sensitive to the accuracy of POD orbit estimates, as long as the spectral characteristics of the time-dependent orbit error are dominated by 1-cpr variability and a long-arc (several orbital periods) orbit error estimation technique is used. The simultaneous solution method was applied to the NAG Geosat data, which have been much maligned in the literature for their low accuracy and unknown spectral characteristics. It has been shown here that the residual time-dependent sea level signals after removal of the mean sea level and sinusoid orbit errors estimated by the long-arc simultaneous solution method are the same, for all practical purposes, in the NAG data as in the much higher quality GEM-T2 data. At longer wavelengths, the energy levels of the differences between the NAG and GEM-T2 sea level residuals can be significant. Studies of large-scale, time-dependent sea level variability are therefore more dependent on the POD accuracy. Studies of the time-invariant sea level associated with the mean ocean circulation are, of course, critically dependent on the POD accuracy (see, for example, *Tai* [1988*a*]).

We conclude with a note of caution regarding the best choice of orbit error estimation method. It must be acknowledged that least squares fits of long arcs of altimeter data to 1-cpr sinusoids isolate only the orbit error problem of time-dependent studies. In this sense, long-arc methods very effectively accomplish their intended goal. However, the 1 cpr fits do not accommodate the shorter scales (thousands of kilometers or less) of other contributions to altimeter measurement errors such as uncertainties in tropospheric and ionospheric corrections for atmospheric refraction, the sea state bias correction, tidal corrections and uncertainty in the "inverted barometer effect" of atmospheric pressure loading. Paradoxically, these other sources of error can be mitigated to some extent by short-arc polynomial orbit error approximations, but only at the expense of less accurate orbit error estimates and a greater risk of oceanographic signal attenuation. Because of the large magnitudes of some of these sources of error in Geosat data, the best orbit error removal scheme will depend upon the specific application (e.g., mesoscale versus large-scale variability). The TOPEX/Poseidon mission has been carefully designed so that the orbit errors will be less than 13 cm and all other sources of measurement error will be less than a few centimeters. A long-arc 1-cpr orbit error estimation technique should therefore be suitable for all applications of TOPEX/Poseidon data. Finally, it should be kept in mind that all orbit error removal techniques (sinusoidal or polynomial fits) also remove much of the large-scale steric sea level variability associated with seasonal hemispheric heating and cooling. Studies of this sea level signal (which is generally of much less interest scientifically than the sea level changes that occur on much shorter spatial scales in association with seasonal variations in the ocean circulation) are critically dependent on the accuracy of orbit estimates.

APPENDIX A: THE GEOSAT NAG ORBITS

The so-called NAG orbits are the operational Geosat orbits produced by the Naval Astronautics Group and applied to the unclassified National Oceanic and Atmospheric Administration (NOAA) geophysical data records (GDRs) released for civilian applications [*Cheney et al.*, 1987, 1988]. They were derived using the orbit determination software described by *Born et al.* [1988]. The gravitational acceleration used in the force model was based on the relatively low resolution GEM-10 gravity model, which is complete

to degree and order 22 with additional selected terms to degree and order 30 [*Lerch et al.*, 1979].

Weaknesses of the NAG model were compensated to some extent by frequent updates of the state vector consisting of initial conditions (satellite position and velocity) and selected model parameters. This was accomplished by a sequence of forward integrations of the force model over 2-day orbit arcs with 1 day of overlap for each successive arc. At the end of each integration, the predicted orbits were adjusted and a new state vector was obtained by a least squares fit to ground-based Doppler tracking data from the four stations of the OPNET tracking network. These tracking stations are poorly distributed geographically; three are in the continental United States and the other is in Hawaii (see Figure 1 of *Haines et al.* [1990]).

The overlap of successive orbit arcs allows flexibility in when to switch from one arc to the next to obtain the estimated orbit height to be removed from the altimeter range measurements. To minimize the effects of discontinuities between successive arcs, the GDRs provided by NOAA use the middle 24 hours of each 2-day arc with breaks located at a maximum latitude, which almost always occurs over land or ice [*Cheney et al.*, 1987, 1988]. The rms accuracy of the NAG orbits has been estimated to be between 300 and 400 cm [*Born et al.*, 1988; *Haines et al.*, 1990].

APPENDIX B: THE GEOSAT GEM-T2 ORBITS

The precise GEM-T2 orbits used in this study were generated by the Goddard Space Flight Center using the GEODYN-II precision orbit determination and parameter estimation software [*Martin et al.*, 1985]. The gravitational acceleration used in the force model was based on the GEM-T2 gravity model, which is complete to degree and order 36 with more than 600 additional selected terms up to degree and order 50 [*Marsh et al.*, 1990*b*]. The GEM-T2 gravity model is far superior to the GEM-10 gravity model used in the NAG orbits (Appendix A) and is the primary reason for the approximate order of magnitude better accuracy of the GEM-T2 orbits.

The procedure followed to generate the GEM-T2 orbits is very similar to that described by *Haines et al.* [1990] to generate the GEM-T1 orbits. The primary difference is the gravity models used in the two orbit estimates; the GEM-T1 model is complete only to degree and order 36 without the additional 600 higher-order terms. Another significant difference is the arc lengths over which the force model was integrated (17 days for the GEM-T1 orbits versus 5–6 days for the GEM-T2 orbits). A detailed description of the GEM-T2 orbits is given by Haines et al. (submitted).

The complex atmospheric drag and radiation pressure forces in the POD force model are approximated in the GEODYN-II software through the use of simplified satellite form modeling. For example, in the force model computations on Geosat, the satellite was treated as a sphere. Depending on the air density, such simplifications can result in large orbit errors. Presently available drag models incorporate orbital information only for satellites lower than 700-km altitude. The air density values at the 800-km Geosat orbit altitude are computed based upon extrapolations within the drag model and can consequently be highly uncertain. This is particularly true during periods of high solar activity. High and variable solar activity induces rapid changes in air density at high altitudes as the atmosphere expands and contracts. Periods of high solar activity were experienced intermittently during the early period of the Geosat mission and persistently throughout the latter period of the mission (see Figure 5*a*).

Orbit errors introduced by errors in the POD force modeling will be greatly reduced for TOPEX/Poseidon. Atmospheric drag is less important by a factor of 2 or more at the higher 1300-km altitude because of the much lower air density. In addition, an improved model for the solar radiation pressure and drag effects that accommodates variations in the cross-sectional area of the satellite in the Sun, Earth, and velocity-pointing directions and that accounts for direct solar and albedo effects, has been developed for TOPEX/Poseidon.

To compensate for much of the secular error in Geosat orbit accuracy incurred during the period of each orbit arc, the coupling coefficients for drag and radiation pressure forces in the force model were adjusted periodically during each arc as part of the least squares adjustment to the tracking data. For the GEM-T2 orbits, the state vector included drag coefficients for each 24-hour period and a single solar radiation pressure coefficient for each 5- to 6-day orbit arc. Whenever possible, the drag coefficient adjustments were made for 24-hour intervals beginning at 0000 UT; depending on the timing of the orbit arc boundaries, the first and last drag coefficient adjustments of each arc may have occurred at times other than 0000 UT, resulting in periods somewhat shorter or longer than 24 hours between drag coefficient adjustments at the ends of the orbit arcs.

Successive GEM-T2 orbit arcs overlap by 1–2 days. As with the NAG data described in Appendix A, the overlapping GEM-T2 orbit arcs were broken at a maximum latitude for the data used in this study, resulting in data arcs generally between 5 and 6 days in duration with some arcs as short as 4 days. The rms accuracy of the GEM-T2 orbits has been estimated as between 30 and 50 cm during the first 2 years of the Geosat Exact Repeat Mission (Haines et al., submitted).

Acknowledgments. We thank Richard Rapp and Yan Ming Wang for providing the first year of GEM-T2 Geosat data and Victor Zlotnicki and Akiko Hayashi for providing the second year of GEM-T2 data and the NAG Geosat data used in this study. This study benefitted greatly from the interest and input of a large number of individuals, which perhaps reflects the importance of the orbit error problem in satellite altimetry. We are grateful to Richard Coleman for many helpful general discussions of gravity fields and orbit determination during the early stages of this work; to Bruce Douglas, Steve Klosko, John Robbins, and Victor Zlotnicki for their help and patience explaining the physical basis for m-daily gravity-induced perturbations in satellite orbits; to Victor Zlotnicki for first suggesting the daily drag coefficient adjustment in the GEM-T2 precision orbit determination procedure as a cause of the daily modulation of 1-cpr orbit error discussed in section 4.2; to Bruce Haines and Steve Klosko for explaining the details of the daily drag coefficient adjustment procedure; to Carl Wagner for drawing our attention to the existence of daily variations in the mean orbit error discussed in section 4.3; and to Richard Rapp and other members of the TOPEX/Poseidon orbit determination team for offering helpful suggestions for interpretation of the results of this analysis. We also acknowledge many helpful comments on the manuscript (the cumulative sum of which exceeded the length of the manuscript) from Bruce Haines, Kathie Kelly, Steve Klosko, C. K. Shum, Carl

Wagner, Donna Witter, and Carl Wunsch. Part of this analysis was conducted while one of the authors (D.B.C.) was a visiting scientist at the CSIRO Marine Laboratories in Hobart, Tasmania. We wish to express gratitude to the CSIRO Division of Oceanography and to John Church in particular for their generous hospitality and the use of CSIRO facilities. This research was supported by contract 958127 from the Jet Propulsion Laboratory funded under the TOPEX Announcement of Opportunity.

REFERENCES

Anderle, R. J., and R. L. Hoskin, Correlated errors in satellite altimeter orbits, *Geophys. Res. Lett.*, *4*, 421–423, 1977.

Born, G. H., F. G. Lemoine, and M. J. Crawford, Geosat ERM–Orbit determination, *Adv. Astronaut. Sci.*, *65*, 65–81, 1988.

Brenner, A. C., C. J. Koblinsky, and B. D. Beckley, A preliminary estimate of geoid-induced variations in repeat orbit satellite altimeter observations, *J. Geophys. Res.*, *95*, 3033–3040, 1990.

Cartwright, D. E., and R. D. Ray, Oceanic tides from Geosat altimetry, *J. Geophys. Res.*, *95*, 3069–3090, 1990.

Caruso, M. J., Z. Sirkes, P. J. Flament, and M. K. Baker, Altimeter processing tools for analyzing mesoscale ocean features, *Tech. Rep. WHOI-90-25*, 200 pp., Woods Hole Oceanogr. Inst., Woods Hole, Mass., 1990.

Chelton, D. B., WOCE/NASA Altimeter Algorithm Workshop, *U.S. WOCE Tech. Rep. 2*, 70 pp., U.S. Planning Office for WOCE, College Station, Tex., 1988.

Chelton, D. B., E. J. Walsh, and J. L. MacArthur, Pulse compression and sea level tracking in satellite altimetry, *J. Atmos. Oceanic Technol.*, *6*, 407–438, 1989.

Chelton, D. B., M. G. Schlax, D. L. Witter, and J. G. Richman, Geosat altimeter observations of the surface circulation of the Southern Ocean, *J. Geophys. Res.*, *95*, 17,877–17,903, 1990.

Cheney, R. E., and J. G. Marsh, Oceanic eddy variability measured by GEOS-3 altimeter crossover differences, *Eos Trans. AGU*, *62*, 737, 743, 1981.

Cheney, R. E., and L. Miller, Recovery of sea level signal in the western tropical Pacific from Geosat altimetry, *J. Geophys. Res.*, *95*, 2977–2984, 1990.

Cheney, R. E., J. G. Marsh, and B. D. Beckley, Global mesoscale variability from repeat tracks of Seasat altimeter data, *J. Geophys. Res.*, *88*, 4343–4353, 1983.

Cheney, R. E., B. C. Douglas, R. W. Agreen, L. Miller, and D. L. Porter, Geosat altimeter geophysical data record (GDR) user handbook, *NOAA Tech. Memo. NOS NGS-46*, 29 pp., Natl. Ocean Surv., Rockville, Md., March 1987.

Cheney, R. E., B. C. Douglas, R. W. Agreen, L. Miller, and N. S. Doyle, The NOAA Geosat geophysical data records: Summary of the first year of the Exact Repeat Mission, *NOAA Tech. Memo. NOS NGS-48*, 20 pp., Natl. Ocean Surv., Rockville, Md., Sept. 1988.

Cheney, R. E., W. J. Emery, B. J. Haines, and F. J. Wentz, Recent improvements in Geosat altimeter data, *Eos Trans. AGU*, *72*, 577, 579–580, 1991.

Cleveland, W. S., and S. J. Devlin, Locally weighted regression: An approach to regression analysis by local fitting, *J. Am. Stat. Assoc.*, *83*, 596–610, 1988.

Colombo, O. L., Altimetry, orbits and tides, *NASA Tech. Memo. 86280*, 173 pp., 1984.

Colombo, O. L., The dynamics of global positioning system orbits and the determination of precise ephemerides, *J. Geophys. Res.*, *94*, 9167–9182, 1989.

Denker, H., and R. H. Rapp, Geodetic and oceanographic results from the analysis of 1 year of Geosat data, *J. Geophys. Res.*, *95*, 13,151–13,168, 1990.

Douglas, B. C., and P. D. Gaborski, Observation of sea surface topography with GEOS-3 altimeter data, *J. Geophys. Res.*, *84*, 3893–3896, 1979.

Douglas, B. C., and C. C. Goad, The role of orbit determination in satellite altimeter data analysis, *Boundary Layer Meteorol.*, *13*, 245–251, 1978.

Engelis, T., On the simultaneous improvement of a satellite orbit and determination of sea surface topography using altimeter data, *Manuscr. Geod.*, *13*, 180–190, 1988.

Gorney, D. J., Solar cycle effects on the near-earth space environment, *Rev. Geophys.*, *28*, 315–336, 1990.

Haines, B. J., G. H. Born, G. W. Rosborough, J. G. Marsh, and R. G. Williamson, Precise orbit computation for the Geosat Exact Repeat Mission, *J. Geophys. Res.*, *95*, 2871–2885, 1990.

Kaula, W. M., *Theory of Satellite Geodesy*, 124 pp., Blaisdell, Waltham, Mass., 1966.

Kelly, K. A., T. M. Joyce, D. M. Schubert, and M. J. Caruso, The mean sea surface height and geoid along the Geosat subtrack from Bermuda to Cape Cod, *J. Geophys. Res.*, *96*, 12,699–12,709, 1991.

Lerch, F. J., S. M. Klosko, R. E. Laubscher, and C. A. Wagner, Gravity model improvement using GEOS-3 (GEM-9 and 10), *J. Geophys. Res.*, *84*, 3897–3915, 1979.

Le Traon, P. Y., M. C. Rouquet, and C. Boissier, Spatial scales of mesoscale variability in the North Atlantic as deduced from Geosat data, *J. Geophys. Res.*, *95*, 20,267–20,285, 1990.

Le Traon, P. Y., C. Boissier, and P. Gaspar, Analysis of errors due to polynomial adjustment of altimeter profiles, *J. Atmos. Oceanic Technol.*, *8*, 385–396, 1991.

Marsh, J. G., and R. G. Williamson, Precision orbit analyses in support of the Seasat altimeter experiment, *J. Astronaut. Sci.*, *28*, 345–369, 1980.

Marsh, J. G., C. J. Koblinsky, F. Lerch, S. M. Klosko, J. W. Robbins, R. G. Williamson, and G. B. Patel, Dynamic sea surface topography, gravity, and improved orbit accuracies from the direct evaluation of Seasat altimeter data, *J. Geophys. Res.*, *95*, 13,129–13,150, 1990*a*.

Marsh, J. G., et al., The GEM-T2 gravitational model, *J. Geophys. Res.*, *95*, 22,043–22,071, 1990*b*.

Martin, T. V., W. F. Eddy, D. D. Rowlands, and D. E. Pavlis, GEODYN system description, contractor report, 5 volumes, 800 pp., EG&G Washington Anal. Serv. Cent., Lanham, Md., 1985.

Rapp, R. H., GEOS-3 data processing for the recovery of geoid undulations and gravity anomalies, *J. Geophys. Res.*, *84*, 3784–3792, 1979.

Rapp, R. H., Y. M. Wang, and N. K. Pavlis, The Ohio State 1991 geopotential and sea surface topography harmonic coefficient models, *Rep. 451*, Dep. of Geod. Sci., Ohio State Univ., Columbus, Aug. 1991.

Rummel, R., and R. H. Rapp, Undulation and anomaly estimation using GEOS-3 altimeter data without precise satellite orbits, *Bull. Geod.*, *51*, 73–88, 1977.

Rosborough, G. W., and J. A. Marshall, Effect of orbit error on determining sea surface variability using satellite altimetry, *J. Geophys. Res.*, *95*, 5273–5277, 1990.

Rosborough, G. W., and B. D. Tapley, Radial, transverse and normal satellite position perturbations due to the geopotential, *Celest. Mech.*, *40*, 409–421, 1987.

Sanchez, B. V., The determination of the orbit of the Japanese satellite "AJISAI" and assessment of the GEM-T1 and GEM-T2 gravity field models, *Manuscr. Geod.*, *16*, 191–204, 1991.

Sanchez, B. V., and D. E. Cartwright, Tidal estimation in the Pacific with application to Seasat altimetry, *Mar. Geod.*, *12*, 81–115, 1988.

Sandwell, D. T., and B. Zhang, Global mesoscale variabilty from the Geosat Exact Repeat Mission: Correlation with ocean depth, *J. Geophys. Res.*, *94*, 17,971–17,984, 1989.

Schlax, M. G., and D. B. Chelton, Frequency domain diagnostics for linear smoothers, *J. Am. Stat. Assoc.*, *87*, 1070–1081, 1992.

Schrama, E., The role of orbit errors in processing of satellite altimeter data, *Publ. on Geod.*, *33*, 167 pp., Neth. Geod. Comm., Delft, 1989.

Shum, C. K., D. N. Yuan, J. C. Ries, J. C. Smith, B. E. Schutz, and B. D. Tapley, Precision orbit determination for the Geosat Exact Repeat Mission, *J. Geophys. Res.*, *95*, 2887–2898, 1990.

Sirkes, Z., and C. Wunsch, Note on apparent systematic and periodic errors in Geosat orbits, *Geophys. Res. Lett.*, *17*, 1307–1310, 1990.

Tai, C.-K., Estimating the basin-scale ocean circulation from satellite altimetry, I, Straightforward spherical harmonic expansion, *J. Phys. Oceanogr.*, *18*, 1398–1413, 1988*a*.

Tai, C.-K., Geosat crossover analysis in the tropical Pacific, 1, Constrained sinusoidal crossover adjustment, *J. Geophys. Res.*, *93*, 10,621–10,629, 1988*b*.

Tai, C.-K., Accuracy assessment of widely used orbit error approximations in satellite altimetry, *J. Atmos. Oceanic Technol.*, *6*, 147–150, 1989.

Tai, C.-K., How to observe the gyre to global-scale variability in satellite altimetry: Signal attenuation by orbit error removal, *J. Atmos. Oceanic Technol.*, *8*, 272–288, 1991.

Tapley, B. D., Fundamentals of orbit determination, in Theory of Satellite Geodesy and Gravity Field Determination, edited by F. Sansò and R. Rummel, *Lecture Notes in Earth Sciences*, vol. 25, pp. 235–260, Springer-Verlag, New York, 1989.

Tapley, B. D., and G. W. Rosborough, Geographically correlated orbit error and its effect on satellite altimetry missions, *J. Geophys. Res.*, *90*, 11,817–11,831, 1985.

Tapley, B., B. Schutz, J. Ries, and C. Shum, Precision orbit determination for TOPEX/Poseidon, *Adv. Space Res.*, *10*, 239–247, 1990.

van Gysen, H., R. Coleman, R. Morrow, B. Hirsch, and C. Rizos, Analysis of collinear passes of satellite altimeter data, *J. Geophys. Res.*, *97*, 2265–2277, 1992.

Wagner, C. A., Radial variations of a satellite orbit due to gravitational errors: Implications for satellite altimetry, *J. Geophys. Res.*, *90*, 3027–3036, 1985.

Wagner, C. A., Summer school lectures on satellite altimetry, in Theory of Satellite Geodesy and Gravity Field Determination, edited by F. Sansò and R. Rummel, *Lecture Notes in Earth Sciences*, vol. 25, pp. 285–334, Springer-Verlag, New York, 1989.

Wagner, C. A., The M_2 tide from Geosat altimetry, *Manuscr. Geodet.*, *15*, 283–290, 1990.

Wunsch, C., Global-scale sea surface variability from combined altimetric and tide gauge measurements, *J. Geophys. Res.*, *96*, 15,053–15,082, 1991.

Zlotnicki, V., L.-L. Fu, and W. Patzert, Seasonal variability in global sea level observed with Geosat altimetry, *J. Geophys. Res.*, *94*, 17,959–17,969, 1989.

Zlotnicki, V., A. Hayashi, and L.-L. Fu, The JPL-Oceans 8902 version of Geosat altimetry data, *Rep. JPL D-6939*, 17 pp. plus figures, Jet Propul. Lab., Pasadena, Calif., March 1990.

D. B. Chelton and M. G. Schlax, College of Oceanic and Atmospheric Sciences, Oregon State University, Oceanography Administration Building 104, Corvallis, OR 97331-5503.

(Received April 30, 1992;
revised December 29, 1992;
accepted February 19, 1993.)